A voyage planning framework for energy performance analysis of autonomous inland waterway vessels

Energy 335 (2025) 137906

Contents lists available at ScienceDirect

Energy

journal homepage: www.elsevier.com/locate/energy

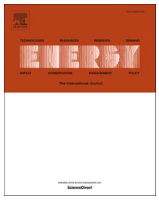

A voyage planning framework for energy performance analysis of autonomous inland waterway vessels

Chengqian Zhang [a,*], Chi Zhang [a], Fabian Thies [b], Wengang Mao [a], Jonas W. Ringsberg [a]

[a] Division of Marine Technology, Department of Mechanics and Maritime Sciences, Chalmers University of Technology, Gothenburg, Sweden
[b] FRIENDSHIP SYSTEMS AG, Potsdam, Germany

ARTICLE INFO

Handling Editor: X Ou

Keywords:
Autonomous vessels
Energy efficiency
Fuel consumption optimisation
Inland shipping
Operational analysis
River hydraulics

ABSTRACT

Autonomous inland waterway vessels (AIWVs) have emerged as a promising solution towards sustainable and intelligent waterborne transport. However, the unique constraints of inland waterways—such as limited manoeuvring space, shallow depth profiles, and water currents pose significant challenges for vessels' navigational safety and energy efficiency. This study aims to develop and validate a simulation framework for energy-efficient autonomous vessel operations in complex inland waterways. To enhance shipping automation with optimal energy usage, this study presents the development of a novel, holistic voyage planning framework (VPF) specifically designed for inland waterway vessels to support both quantitative energy performance assessment and operational analysis. The operations of AIWVs are systematically examined, including ship design (energy performance modelling), manoeuvring modelling, control design, and energy prediction under various inland waterway scenarios. To capture the impact of riverbed topography on ship manoeuvrability and propulsion energy demand in meandering waterways, a new formula is proposed to model river hydraulics, incorporating cross-sectional shifts, current fields, deposition, and erosion effects. Several case studies are conducted under different operational modes to demonstrate the capability of the VPF to enable robust path-following control, dynamic energy prediction, and fuel consumption optimisation. The simulation results indicate that up to 5.7 % fuel savings can be achieved during near-bank operations in shallow water through operational speed optimisation. The proposed VPF can help to improve vessel operational efficiency and reduce energy consumption in confined inland waterways. Moreover, the findings can serve as a digital testbed for evaluating new vessel designs and retrofitting strategies aimed at enhancing automation and energy performance.

1. Introduction

Shifting cargo from roads to inland waterways is a promising solution for achieving a more sustainable mode of transport, as it helps reduce CO2 emissions [1,2]. With increasing levels of autonomy and advances in sensor technology, autonomous inland waterway vessels (AIWVs) are regarded as key components in developing intelligent waterborne transport networks. These vessels can enhance logistics by reducing crew requirements and operational costs while improving safety.

Given the distinct nature of inland waterways, where rivers and channels are typically constrained by water depth and width, it is particularly important to investigate vessel dynamics and energy consumption to ensure operational safety and efficiency. In particular, route feasibility assessment, path-following simulation, and accurate energy prediction that accounts for interactions between the vessel and surrounding environmental constraints (e.g. banks, currents, and infrastructure) are essential for realistic evaluations of autonomous operations. Based on these results, energy consumption can be further optimised for AIWVs along different routes, enabling more sustainable and intelligent operations.

While AIWVs share conceptual similarities with autonomous road vehicles, their operation in dynamic water environments presents additional challenges, including time-varying hydrodynamic forces, spatial constraints, and delayed vessel responses due to large inertia and slow steering dynamics. This makes proactive control strategies essential for ensuring safe and efficient navigation, especially for full-scale autonomous vessels.

* Corresponding author.
E-mail addresses: chengqian.zhang@chalmers.se (C. Zhang), chizha@chalmers.se (C. Zhang), thies@friendship-systems.com (F. Thies), wengang.mao@chalmers.se (W. Mao), jonas.ringsberg@chalmers.se (J.W. Ringsberg).

https://doi.org/10.1016/j.energy.2025.137906
Received 27 May 2025; Received in revised form 3 August 2025; Accepted 4 August 2025
Available online 7 August 2025

These challenges highlight the need for a dedicated simulation framework to analyse vessel energy performance under dynamic operations, especially steering in meandering inland waterways where hydrodynamic interactions strongly influence control behaviour and energy efficiency. Accurate modelling and realistic assessment of autonomous operations in confined waterways require a clear understanding of the associated navigational challenges and the key physical and operational factors that influence inland vessel behaviour, particularly including hydrodynamic modelling, control design, and energy performance evaluation.

1.1. Navigational challenges

Navigation in inland waters presents distinct challenges due to fairway constraints such as shallow depth, narrow width, and the presence of artificial infrastructure like bridges, locks, and terminals. These factors lead to confined operational environments, where vessels experience additional hydrodynamic loads from shallow water [3–5] and channel banks [6], adversely affecting manoeuvrability [7,8] and energy efficiency [9–12]. A vessel operating at an unfavourable speed range in confined waters can significantly increase resistance and propulsion power demand.

In addition, hydrological factors, such as dynamic water currents, curvature of the channel, and riverbed morphological changes, further influence vessel performance [13]. Yang et al. [14] showed that a vessel's hydrodynamic performance becomes more complex in curved channels, with ship handling highly sensitive to channel geometry and current velocity. At river bends, secondary flows cause erosion of the outer bank and deposition along the inner bank, forming point bars and leading to lateral migration of the riverbed. This results in a more complicated operational environment, as navigation at river bends involves asymmetric hydrodynamic forces—vessels on the outer side may require more substantial steering corrections, while the inner side poses grounding risks due to sedimentation and reduced depth.

Given the presence of these factors affecting vessel energy efficiency, along with other environmental disturbances that influence vessel handling, the operational performance of AIWVs should be carefully examined by analysing vessel dynamics under these conditions.

1.2. Related work

As outlined in the previous section, the development of simulation frameworks for AIWVs relies on a solid understanding of hydrodynamic behaviour, control strategies, and energy consumption patterns. This section reviews related literature in these areas and identifies key limitations that motivate the development of the proposed framework for autonomous vessels operating in confined waters.

1.2.1. Ship performance in inland waterways

When a ship sails on inland waterways, decreasing water depth leads to significant flow interactions between the ship's bottom and the riverbed, resulting in increased drag on the hull [3,15]. In addition, the accelerated flow beneath the hull causes a pressure difference, which leads to additional sinkage and increased resistance—commonly known as the squat effect [4]. Over the past decades, numerous studies have employed model tests [16–18] and computational fluid dynamics (CFD) simulations [5,19,20] to quantify shallow-water effects on ship hydrodynamics.

In addition, inland vessels must operate in confined waters, where both vertical and lateral directions are constrained, such as in narrow rivers or canals. A reduced ship-bank distance leads to increased resistance and also induces lateral forces and yaw moments—commonly referred to as the bank effect. Du et al. [18] conducted model tests and CFD studies to evaluate ship resistance under varying channel widths and depths. Mucha et al. [16] also conducted model tests and found that channel walls can cause a noticeable increase in resistance, although the dominant hydrodynamic effects are lateral forces and yaw moments.

1.2.2. Manoeuvring and control design

Ship manoeuvring is a critical consideration for inland vessels. Beyond changes in resistance, shallow-water effects also have a significant impact on side forces and yaw moments acting on the hull, which in turn affect the vessel's manoeuvring behaviour [7,21,22]. In confined waters, additional lateral forces from channel walls or nearby infrastructure further complicate the prediction of vessel motion. Existing studies [8,21,23] show that a key challenge is that conventional manoeuvring models—such as the Nomoto model [24], the whole ship model [25], and the modular manoeuvring group (MMG) model [26]—were developed for open-water conditions and may not be suitable for inland waterways due to the distinct operational environment.

In response, a series of studies have sought to improve manoeuvring models for shallow and confined waters. Yoshimura [27] applied hydrodynamic derivatives of a car carrier in shallow water to the original MMG model and validated the results under various water depths. However, the vessel used to generate the data had a hull form that differed significantly from that of an inland vessel, limiting its applicability. Liu et al. [28] proposed a manoeuvring model tailored for inland vessels, though it was still applied in deep water, neglecting confined-water effects. More recently, Yang and el Moctar [29] improved the Abkowitz model by incorporating shallow-water correction terms derived from extensive captive model tests. These tests, conducted using an inland vessel under varying water depths, were successfully validated in full-scale trials of an inland barge. Similarly, Zhang et al. [30] proposed a modified MMG model that accounts for both shallow-water and bank effects.

Overall, while manoeuvring modelling in confined water has improved over the past decade, its application remains limited—often restricted to model validation such as comparisons of turning circles. These mathematical models should be further leveraged in operational analyses of vessel behaviour under complex river bathymetries.

Control design is another vital task for inland vessels, especially for AIWVs, as precise path-following control is essential to ensure navigational safety under complex environmental disturbances in restricted operational spaces [31,32]. A vessel navigating river bends must frequently adjust its heading and correct for drift. Under disturbances such as current and hydrodynamic loads in confined water, a robust control scheme is required for effective course-keeping along curved paths.

Chen et al. [33] proposed a distributed model predictive control (MPC) method for vessel platooning operations, demonstrating good results during port navigation in deep-water regions. Similarly, Tao et al. [34] developed an MPC-based framework for vessel platooning control in inland waters, though the vessel dynamics and environmental forces were still overly simplified. Xu et al. [35] improved heading control for large inland vessels in confined water using MPC on a simplified MMG model with experimentally derived hydrodynamic coefficients. However, the application was limited to straight channels, and shallow-water resistance was not considered.

From existing research, it can be seen that model-based control algorithms [33,36–38] have shown promise in congested waters, but they often rely on overly simplified manoeuvring models. Moreover, their application is typically confined to ports or straight channels, with limited consideration of waterway bathymetry—raising concerns about their suitability for natural rivers.

As the environment becomes more complex, the non-linear effects encountered during long voyages require significant computational effort, which can affect MPC performance. Although linear MPC can offer computational benefits, linearising vessel dynamics in curved waterways remains challenging and requires comprehensive system identification. To enhance the robustness of heading control under the complex conditions of inland navigation, some researchers have proposed reinforcement learning approaches [32,39]. These methods can

improve control performance, but they also entail high training and computational costs.

It can be concluded that research on ship manoeuvring and control in confined water has primarily focused on methodology rather than practical applications, for example, pure manoeuvring modelling without vessel control simulation, or the development of sophisticated control methods based on oversimplified vessel dynamics and environmental conditions. For AIWVs, high-fidelity manoeuvring and hydrodynamic models integrated with control algorithms are crucial to support realistic and reliable remote or autonomous operations.

1.2.3. Energy efficiency

Beyond hydrodynamics and motion control, ship energy efficiency is a key indicator of sustainable transport and logistics on inland waterways [40–43]. As environmental regulations become increasingly strict and fuel costs rise, reducing energy consumption has become both an economic and ecological priority for improving the competitiveness of inland waterway shipping. Although the Energy Efficiency Design Index (EEDI) is widely used for seagoing vessels, researchers [44,45] indicated it does not sufficiently account for the unique environmental and operational characteristics of inland water transport, which motivates the need for improving inland-specific energy efficiency methodologies or frameworks, as existing indices such as the EEDI are not well-suited for inland navigation [45]. This section reviews current methods, technologies, and strategies for predicting and enhancing energy efficiency in inland waterway vessels.

An inherent feature of inland vessels is that propulsion power is sensitive to waterway conditions. Hence, an accurate method for dynamic power prediction is important for energy efficiency analysis. Zhang et al. [10] proposed a physics-based ship performance model for predicting the propulsion power and fuel consumption of inland vessels, and the results showed good agreement with both experimental and full-scale measurements. Fan et al. [46] evaluated various machine learning models for predicting ship energy consumption using onboard sensor data from an inland bulk carrier and concluded that Random Forest and XGBoost provided the best predictions.

In addition to energy consumption prediction, emission modelling [47] is also vital for evaluating energy efficiency. Fan et al. [48] used onboard measurements from two Yangtze River ships to assess how operational parameters and fuel type affect emissions, showing that optimised controls can reduce emissions. The impact of fuel selection is also discussed, as the use of liquefied natural gas (LNG) can increase CO emissions, even though it helps to reduce CO2 and NOx emissions. Furthermore, Fan et al. [49] developed a micro-macro model to assess the carbon footprint of inland shipping, where low-carbon pathways for inland ships were proposed.

With the development of various energy prediction methods, studies on energy efficiency optimisation have been actively conducted. Wang et al. [50] reviewed CFD-based ship energy-saving technologies, showing that hull and propeller optimisation can effectively reduce energy consumption. Yuan et al. [51] proposed a data-driven model for fuel consumption estimation of an inland vessel, and a heuristic optimisation algorithm was used to optimise engine speed to minimise fuel consumption and operational costs. Wang et al. [42] integrated a wavelet neural network to predict short-term working conditions alongside a real-time engine speed optimisation model on a river cruise vessel. Yan et al. [41] used big data analytics and a distributed k-means clustering algorithm to segment inland ship routes and determine optimal engine speeds under varying environmental conditions. Similarly, Perera and Mo [52] proposed a machine intelligence-based framework that combines onboard data pre-processing with shore-based analysis to enhance ship performance data for energy efficiency management. These studies provide a valuable foundation for energy efficiency optimisation in autonomous vessels, where accurate energy prediction and optimisation are essential for supporting autonomous decision-making under varying operational and environmental conditions.

However, current research on vessel energy efficiency relies heavily on data measurement. For future autonomous vessels, such data is normally very limited or unavailable during the early design stage, which significantly affects the generalisation ability of these machine learning-based approaches.

1.3. Contributions of this study

From the literature review in the previous sections, it can be concluded that a systematic approach to the energy performance analysis of inland vessels is missing. To evaluate the operational performance of AIWVs, ship energy consumption prediction, manoeuvring and control design should be integrated within a comprehensive framework. A vital requirement of such a system is that these sub-models must capture the distinct physical conditions of inland waterways, such as shallow water effect, bank effect, and river hydraulics (channel morphology and water currents). Accurate trajectory and attitude prediction based on these models enables dynamic verification of route feasibility, which is essential for reducing the risks of off-track deviation and collision.

Simulation platforms, such as marine simulators, are a popular research area in the maritime industry. Existing studies on simulation platforms are primarily developed for standard commercial vessels operating in open-sea conditions [53–55]. The voyage plan is executed and monitored using a built-in electronic chart display and information system (ECDIS). While these advanced simulation platforms are well developed for commercial shipping, most do not account for the specific conditions of inland waterways.

The inland ECDIS is relatively new and has been continuously developed over the past decades (CCNR, 2014). However, extracting detailed river profile information is often challenging, as ECDIS is typically integrated into built-in software. Moreover, these commercial simulators are usually complex and include numerous features, making them less suitable for research purposes.

These limitations highlight the lack of accessible and flexible tools for inland waterway research. Commercial simulators and ECDIS systems are primarily designed for training or operational support in open-sea applications, and their closed architecture and limited adaptability make them unsuitable for rapid testing and development of autonomous inland vessel strategies.

To address this gap, this study aims to develop a novel and efficient voyage planning framework (VPF) designed explicitly for AIWVs. The VPF offers a holistic approach, enabling the evaluation of vessel energy performance from the early design to the operational stages. It is designed as a modular framework, allowing components to be modified or replaced based on the availability and fidelity of data at different development phases. A key feature of the platform is a novel hydraulic model that allows for the rapid generation of arbitrary inland waterways for simulation analysis. By integrating manoeuvring, control, and energy system performance models, this framework enables the simulation of AIWVs' navigation performance in various inland waterways and provides rapid energy consumption predictions.

The main contributions of this study are summarised as follows.

1) A comprehensive and integrated VPF was developed, which includes energy performance modelling, manoeuvring modelling, control design, and energy efficiency analysis.
2) A novel parametric hydraulic model was proposed, capable of rapidly generating arbitrarily shaped meandering waterways, enabling realistic and flexible simulation environments for autonomous navigation testing.
3) Comprehensive model validation was performed, with a particular focus on the accuracy of energy prediction using actual measurements from various inland vessels. The results demonstrated good agreement with the measured data.

4) Systematic operational analysis for AIWVs was conducted, including energy prediction during vessel control simulation and energy performance optimisation.

The remainder of this paper is structured as follows: Section 2 introduces the development of the VPF, including the ship energy performance modelling, manoeuvring modelling, control design and river generation. In particular, this section proposes a dedicated energy optimisation method tailored for inland waterway operations. Section 3 presents the validation study, focusing on the validation of key models such as the energy performance model and the proposed hydraulic model using experimental data and literature benchmarks. Section 4 describes the vessel operational simulation and energy performance analysis under various scenarios. Section 5 shows the optimisation result for vessel energy consumption in confined waterways. Finally, Section 6 summarises the key findings and provides suggestions for future work.

2. Development of the VPF for inland vessels

This section presents the architecture of the VPF designed for inland vessels. As shown in Fig. 1, the framework comprises several key models and components that collectively represent the essential physical characteristics of vessel dynamics, as well as the influence of the surrounding environment. The ship simulation module has two main objectives: (a) updating the vessel motion based on environmental inputs and control commands, and (b) predicting dynamic propulsion power based on vessel states (e.g., speed, water depth, ship-bank distance). The environment module includes a hydraulic model for bathymetry modelling with current field initialisation. Combined with the ship simulation module, a waterway map is generated and fed into the main voyage planner. After defining the route and engine operational mode, path-following simulations are carried out. The results: vessel trajectories and energy consumption, are analysed in the route analysis module. Based on predicted fuel consumption at each waypoint, an optimisation module can adjust the vessel speed to minimise energy consumption under varying environmental conditions. The detailed interaction between these modules and the sub-models is presented in Fig. 2.

The framework enables a comprehensive analysis of vessel behaviour under various operational scenarios by capturing the interactions among the sub-models. This allows the simulation to assess key performance indicators such as manoeuvrability, path-following accuracy, and energy efficiency of a virtual autonomous inland vessel. The remainder of this section presents the development of these sub-models.

2.1. Energy performance model

The primary function of the ship energy system performance model is to provide rapid feedback on energy consumption by formulating the speed-power relationship. Such a model is essential for autonomous systems, as it enables the monitoring of dynamic energy demand during navigation—a prerequisite for the optimal utilisation of fuel or electricity. However, predicting the energy consumption of autonomous vessels is challenging, particularly in the early design stage, when available information and parameters are very limited. In the previous study [10], a physics-based ship performance model, ShipCLEAN-IWV, was developed to establish the energy system of inland vessels, as shown in Fig. 3.

This model is based on semi-empirical and analytical formulas describing various energy consumption components. The resistance prediction includes a modified formula to account for the impact of shallow water and banks on inland waters, followed by ducted-propeller design and engine modelling. The total fuel consumption rate at speed V_S under specific operational conditions can be calculated using the following equation:

$$FC = SFOC\left(0.5\rho_{FW}S_W C_T V_S^2 + R_S + R_{BANK}\right)\frac{V_S}{(\eta_H\eta_O\eta_R\eta_S)} \quad (1)$$

where $SFOC$ is the specific fuel oil consumption rate, derived from regression methods [56], ρ_{FW} is the freshwater density, S_W is the wetted surface area, C_T is the total resistance coefficient in deep water, R_S is shallow water resistance, R_{BANK} is the bank-induced resistance, V_S is the vessel speed, η_H is the hull efficiency, η_O is the propeller open-water efficiency, η_R is the relative rotative efficiency, and η_S is the shaft transmission efficiency. Detailed information about the performance model is provided in Zhang et al. [10] (see Appendix A).

2.2. Manoeuvring modelling for inland vessels

The manoeuvring model is another critical component of the voyage planning system, as accurate and dynamic updates of vessel motion are essential during navigation. Inland vessels are typically equipped with twin propellers and multiple rudders to ensure adequate manoeuvrability in confined waterways. The coordinate systems used in this

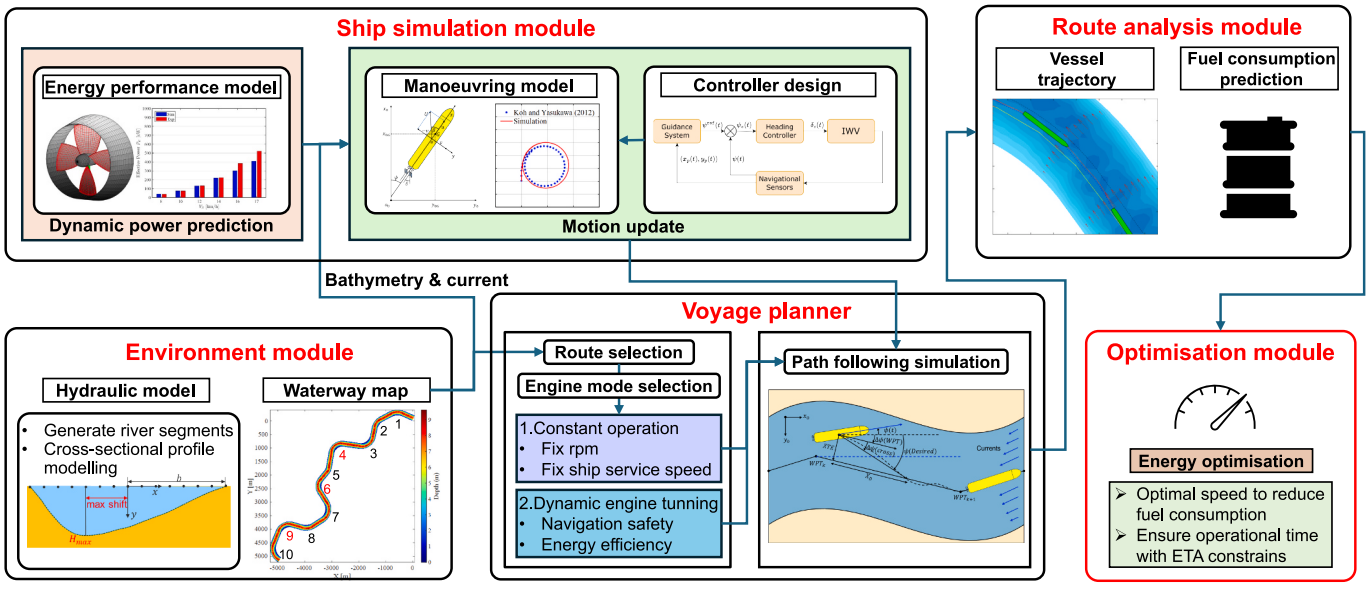

Fig. 1. The architecture of the VPF for AIWVs.

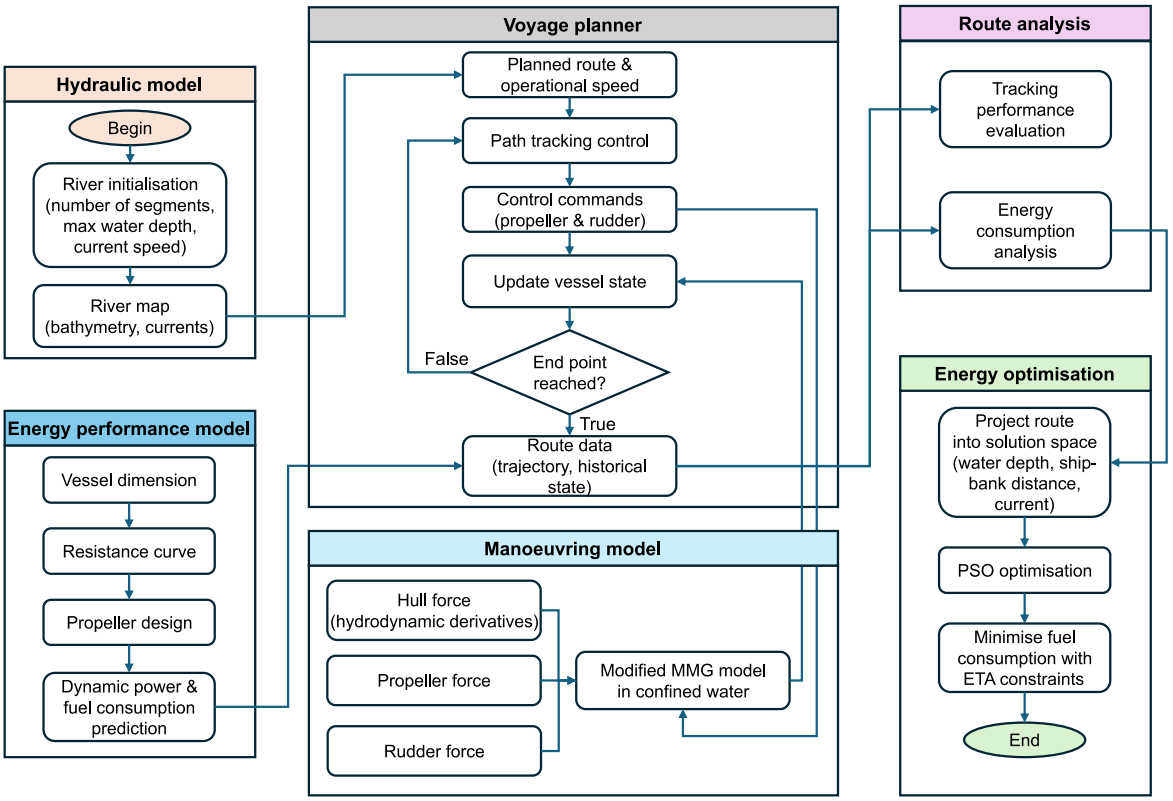

Fig. 2. The detailed flowchart shows the interaction between the sub-models in VPF.

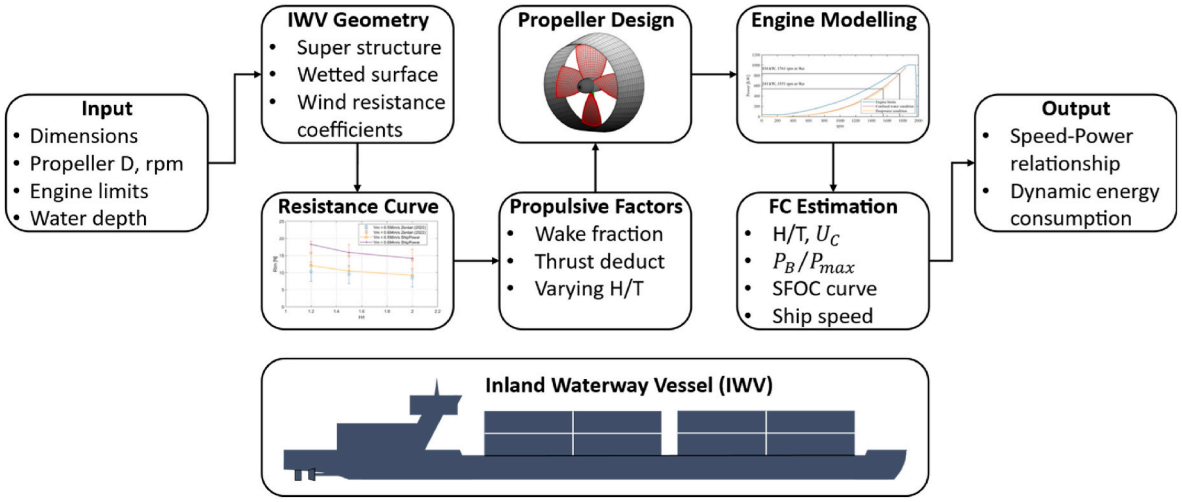

Fig. 3. Overview of the energy performance model ShipCLEAN-IWV, reproduced from Zhang et al. [10].

study are presented in Fig. 4. It is important to note that only two-dimensional (2D) planar ship motion (surge, sway, and yaw) is considered, as inland vessels typically operate in calm water, where vertical motion can be neglected. In the coordinate systems, $o_0 - x_0y_0z_0$ represents the earth-fixed frame, and $o - xyz$ is the body-fixed frame located at midship. G is the centre of gravity (CoG), and u, v_m denote the surge and sway speeds at midship, respectively. It should be noted that u and v_m must be adjusted based on the water's current speed and direction.

Most studies on ship manoeuvring focus on conventional commercial vessels operating in open-water conditions. However, these manoeuvring models may not be directly applicable to inland waterways, as channels and rivers are often constrained by limited width and shallow water depth. Therefore, this study adopts a modified version of the MMG model that includes shallow water and bank effects [30]. The equations of motion are given as:

$$\left.\begin{aligned}(m+m_x)\dot{u} - (m+m_y)v_m r - x_G m r^2 &= X_H + X_P + X_R + X_B\\ (m+m_x)\dot{v}_m + (m+m_x)ur + x_G m\dot{r} &= Y_H + Y_R + Y_B\\ (I_z + x_G^2 m + J_Z)\dot{r} + x_G m(\dot{v}_m + ur) &= N_H + N_R + N_B\end{aligned}\right\} \quad (2)$$

Here, the left-hand side represents the mass m and inertia terms, with I_z, m_x, and m_y denoting the added mass in their respective directions. v_m is the sway speed at mid-ship, and r is the yaw rate. The right-hand side represents forces and moments acting on the ship from different components: sub-scripts H, P, R, and B denote loads from the hull, propeller,

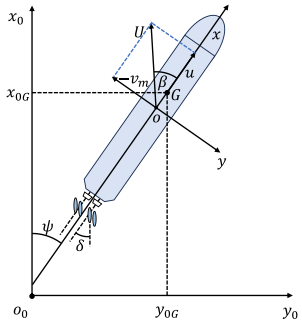

Fig. 4. The coordinate system of an inland vessel.

rudder, and bank effect, respectively. It is important to note that shallow water effects are included in the hull force through corrections to the resistance coefficient and hydrodynamic derivatives. Further details on the hydrodynamic forces acting on the hull, propeller, and rudder of an inland vessel are provided in Zhang et al. [30].

The bank-induced force and bow-out moment are predicted based on three well-known bank effect models [6,57,58]. The detailed parameters and equations can be found in their original studies. The comparison of the lateral force and yaw moment from the three listed methods is presented in Appendix B.

The manoeuvring model was validated using the turning test data of an inland vessel under three different water depth conditions [30]. It should be noted that the bank effect model was directly incorporated into Eq. (2) without trajectory validation, since there are currently no measured, publicly available experimental data for vessel near-bank trajectory validation (the existing studies rely on simulations).

2.3. Guidance and control design

2.3.1. Guidance system

AIWVs require precise control systems to ensure operational safety, as they frequently navigate in confined waterways. In addition to shallow water conditions, river currents can significantly affect course stability. Therefore, the design of the Guidance, Navigation, and Control (GNC) module in this study accounts for these disturbances. The primary objective is to execute effective rudder control to maintain the vessel's heading along predefined waypoints while minimising cross-track error (*XTE*). The schematic of the GNC module for path following under water currents is shown in Fig. 5.

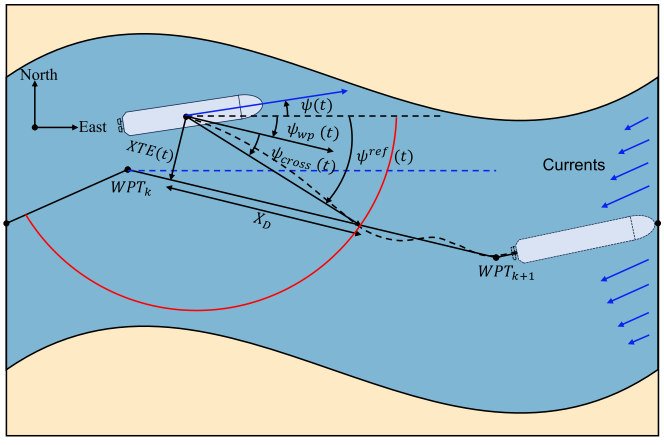

Fig. 5. Schematic of the guidance and heading control in a river meander with water currents.

2.3.2. Rudder control for path tracking

The heading control is implemented based on the Line of Sight (LOS) scheme [59], where the desired heading angle is calculated from the current position and heading. The desired heading angle is determined using the following equation:

$$\psi^{ref}(t) = \psi_{wp}(t) - \psi_{cross}(t) \tag{3}$$

where ψ_{wp} is the angle between the current and next waypoint, serving as the course guidance, and ψ_{cross} is the correction angle used to offset the cross-track error by applying a lookahead distance X_D from a defined circle with a radius of 65 m, as shown by the red arc.

The control design adopts an incremental proportional-integral-derivative (PID) controller to update the rudder angle δ_c. The equation for the rudder angle is:

$$\delta_c(t) = K_p\left((\psi_e(t) - \psi_e(t-1)) + \frac{T_d}{T_s}(\psi_e(t) - 2\psi_e(t-1) + \psi_e(t-2)) + \frac{T_s}{T_i}\psi_e(t)\right) \tag{4}$$

where $\psi_e(t)$ represents the heading error at the current time step t, K_p is the controller's proportional gain, and T_d, T_i, and T_s are the derivative time constant, integral time constant, and sampling period, respectively.

The incremental PID controller differs from the conventional positional PID by computing changes in control input rather than absolute values. This approach offers improved numerical stability and reduced sensitivity to integral windup, which is particularly beneficial in nonlinear dynamic environments [60].

2.4. Hydraulic model

Hydraulic models are crucial for analysing vessel dynamics and energy consumption, especially in confined inland waterways. These models represent key features such as bathymetry profiles, channel geometry, and current fields along meandering waterways [61,62], which are essential for vessel manoeuvring and control design. Most studies focus on developing sophisticated control methods, while the waterway itself is often over-simplified—for example, using straight or uniformly shaped channels with constant water depth. This study presents an improved and more realistic hydraulic model, divided into two parts: (a) waterway generation, which enables the creation of arbitrarily meandering channels, and (b) cross-sectional modelling, which introduces a novel formula for capturing cross-sectional shifts.

2.4.1. River segment generation

An arbitrary meandering river can be generated by combining straight and curved sections of varying sizes [39,63]. This study adopts this method for waterway generation using several segments ($S_1, S_2, \ldots, S_i$), as shown in Fig. 6. Each segment is further divided into a set of cross-sections $c_{i,j}$, created by evenly distributing grid points based on the geometry. The generated rivers are assumed to have a constant width, represented by 15 grid points in the transverse direction, with 15 m spacing between adjacent points, resulting in a total width of 210 m.

Straight segments are defined by a parameter controlling their segment length, except for the first segment, which also includes an

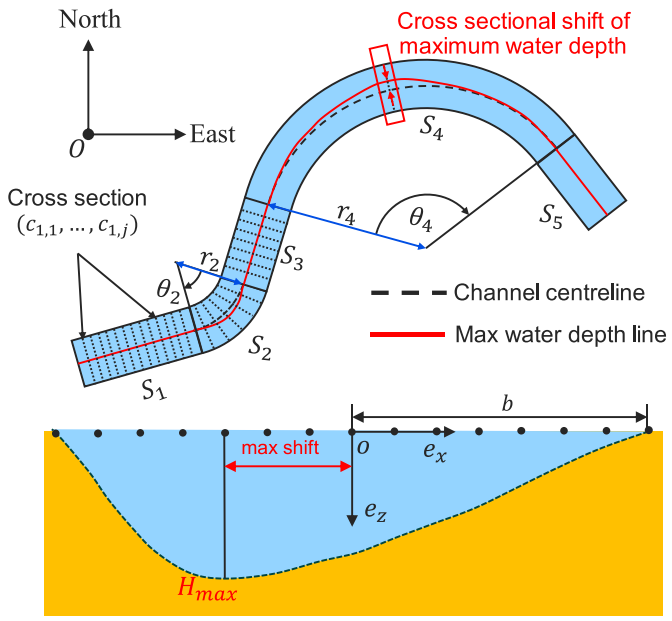

Fig. 6. Demonstration of river generation and cross-sectional profile modelling.

arbitrary starting angle. Curved segments are generated using two variables: the radius r_i and the segmental angle θ_i. Each new segment is transformed to properly attach to and align with the end cross-section of the previous segment, maintaining continuity and geometric consistency.

2.4.2. Cross-section modelling

In existing research, the shape of river cross-sections is typically simplified as rectangular or trapezoidal. The most relevant study is presented in Paulig and Okhrin [39], in which the channel cross-section is modelled using a normal distribution-like formula. However, the maximum depth is assumed to always occur at the river centre, meaning the shift of the riverbed in curved segments is neglected. Additionally, the current field does not account for the impact of bathymetry and waterway geometry. To address this limitation, a parametric formula is proposed to reproduce such cross-sectional asymmetry as a function of curvature, bend radius, and segment location. The depth profile is modelled using the following equation:

$$h_{i,j} = (1 + \varepsilon_h) H_{max} \left(\frac{e_z}{\min(e_z)} \right) \tag{5}$$

where $h_{i,j}$ represents the water depth of cross-section j along the i^{th} segment, ε_h is a random perturbation following a normal distribution with a standard deviation of 0.1, H_{max} is the maximum depth of the cross-section, and e_z represents the shape function of the riverbed in the vertical direction (see Fig. 6) This is calculated using the equation:

$$e_z = -\left(1 - \left(\frac{e_x}{b}\right)^2\right)\left(1 + \gamma_{i,j}\left(\frac{e_x}{b}\right)\right) \tag{6}$$

where e_x is the lateral position in the local frame of each cross-section (see Fig. 6), b is the half-width of the channel, and $\gamma_{i,j}$ is a skewness factor that calculates the cross-sectional shifts depending on the shape of the waterway. This is given as:

$$\gamma_{i,j} = \alpha \left(\frac{\theta_i}{max(\theta)} \right) \left(1 - \left(\frac{\Delta i,j}{(r_i \cdot \theta_i)/2} \right)^2 \right) \tag{7}$$

where α is a constant that decides the direction of the segment curvature ($\alpha \in [-1, 0, 1]$), with 0 for straight segments, negative values if the curvature is towards the left, and vice versa. Further, θ_i is the angle of the segment, $\Delta i,j$ is the arc distance between cross-section j and the mid-section within this segment (as shown in the red box), and r_i is the radius of the segment, as presented in Fig. 6. The equation assumes that the maximum shift occurs in the middle of a curved segment.

2.4.3. Current field

As suggested by Odgaard [62], in river meanders, the distribution of stream velocity in the transverse direction generally follows the corresponding water depth. Therefore, following a similar process as the cross-sectional modelling, the current velocity is formulated to align with the depth profile, enabling a simplified representation of flow asymmetry near bends. The equation for current velocity is:

$$u_{ci,j} = (1 + \varepsilon_c) u_{max} \frac{\left(-\left(1 - \left(\frac{e_x}{b}\right)^2\right)\left(1 + \gamma_{i,j}\left(\frac{e_x}{b}\right)\right)\right)}{\min(e_z)} \tag{8}$$

where U_{max} is the maximum flow velocity, and ε_c is the disturbance, which accounts for uncertainties in flow speed. As a result, the current speed distribution along the transverse direction is nearly parabolic in straight segments. In curved segments, the maximum flow speed is located based on the shifting of the depth profile. The flow direction is assumed to be perpendicular to each cross-section, meaning that vortex or secondary flows cannot be modelled and are thus neglected.

2.5. Energy optimisation

For vessels navigating inland waterways, particularly future autonomous ships, reducing energy consumption is important. For conventional diesel vessels, optimising energy use reduces fuel costs and emissions. For fully electric autonomous ships, optimising energy is vital for extending operational range within limited battery capacity. Optimising speed according to varying operational conditions and environmental factors can significantly reduce fuel or electricity usage, particularly in constrained waterways. This is crucial for enhancing the overall efficiency of waterborne transport. This section introduces the energy optimisation module in the developed VPF, a key functionality that should be incorporated into the onboard automation system for AIWVs.

Due to geographical constraints, the sailing routes of inland vessels are relatively fixed. As a result, the focus of optimisation shifts from path planning to operational mode adjustments, such as speed optimisation along a predefined reference track in response to external environmental conditions. In this work, a Particle Swarm Optimisation (PSO) algorithm is employed to optimise the vessel's speed profile along the target route. PSO is a population-based algorithm [64] that operates using a group of candidate solutions known as particles. These particles collectively form a swarm, where each particle represents a potential solution, and they explore the search space collaboratively. The particles move through the solution space and update their positions over iterations in search of the global optimal.

Fig. 7 demonstrates the main schematic of the PSO algorithm. During the optimisation process, each particle keeps track of two key pieces of information: its best-found position (personal best, $pbest_i^t$) and the best-known position discovered by the swarm (global best, $gbest^t$) at time t. Based on this information, it updates both the velocity and position of the particles. The velocity is adjusted using the particle's own experience and the swarm's shared knowledge, while the new position is calculated based on the current state and the relative distances to both the personal and global bests. The equations are given as:

$$\begin{aligned} V_i^{t+1} &= \omega v_i^t + c_1 r_1 \left(pbest_i^t - x_i^t\right) + c_2 r_2 \left(gbest^t - x_i^t\right) \\ x_i^{(t+1)} &= x_i^t + V_i^{(t+1)} \end{aligned} \tag{9}$$

where ω is the inertia weight for velocity update, c_1 and c_2 are cognitive and social acceleration coefficients, respectively, and r_1 and r_2 are

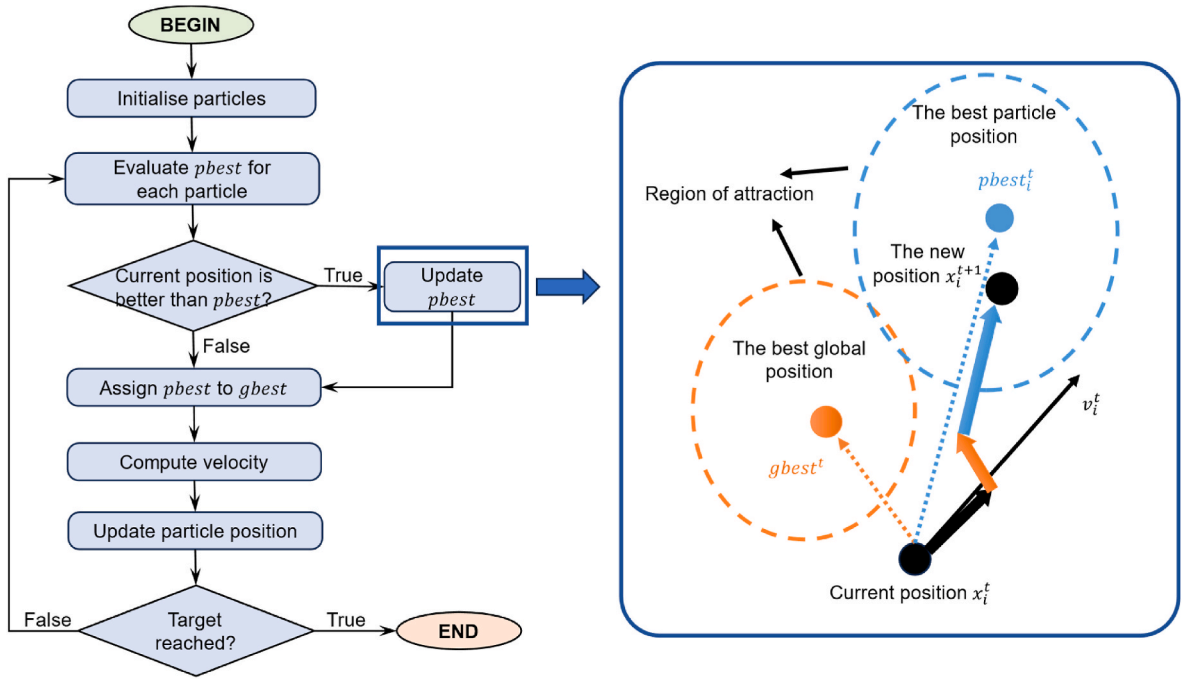

Fig. 7. Schematic of the PSO optimisation process.

random values between [0,1]. $x_i^{(t+1)}$ denotes the updated position of the particle.

Using this method, the sailing route is divided into a series of waypoints. A swam size is then defined, where each particle represents a candidate speed distribution along the route. The aim is to optimise speed selection to minimise fuel consumption while ensuring compliance with estimated time of arrival (ETA) constraints. In the simulation, a dynamic inertia weight is adopted across iterations to enhance convergence towards the global optimum:

$$\omega = \omega_{max} - t((\omega_{max} - \omega_{min})/T) \tag{10}$$

The detailed optimisation process and corresponding results are discussed in Section 5.

2.6. Applicability and limitations of the VPF

The VPF presented in this section is designed with the primary focus on conventional inland vessels. The energy performance modelling is applicable for the classical ship propulsion system with the combination of propeller and diesel/gas engine. It should be noted that the model is not applicable for the performance prediction on other devices, such as hybrid engines, fuel cell systems, or electrical propulsion units.

The manoeuvring model considers the 2D planner motion in three degrees of freedom (3-DoF), and the vertical ship motions are neglected in this study. The modified MMG model includes shallow water correction and bank effect, where the minimum water depth should ensure the depth to vessel draught ratio H/T is larger than 1.2. Water depth below this is regarded as extremely shallow water case and the vessel dynamics cannot be correctly modelled under such conditions. Moreover, the manoeuvring model was developed for single vessel operations, so the multi-vessel conditions with ship-ship interactions were not considered. Heading control was developed for a conventional propeller-rudder system to ensure the effective vessel path following. Other steering units such as azimuth thrusters or tunnel thrusters are not suitable for the proposed rudder controller. During operation, the controller primarily adjusts the rudder angle under fixed propeller speed conditions. Speed control is only activated for specific scenarios when navigation safety must be ensured, such as when passing through bridges or locks.

For the river hydraulics modelling, the proposed equation aims to give a fast prediction on the cross-sectional shift, particularly on the curved segment. More complex phenomena such as sediment transport, nonlinear riverbed evolution, or secondary flow are beyond the capability of this simplified model and require more sophisticated numerical simulations.

3. Model validation

3.1. Validation of energy performance model

This section presents a validation of the energy performance model through simulation, using sensor data from two inland chemical tankers. The predicted power output and fuel consumption rates are verified against field measurements.

3.1.1. Vessel profile

As a continuation of the energy performance model presented in Zhang et al. [10], trial data from two existing inland vessels are used to validate the power prediction and fuel consumption calculations. The data were collected along the Yichang to Zhijiang section of the Yangtze River in China, where the average water depth is approximately 7 m. Vessel 1 is a 3000 DWT chemical tanker, while Vessel 2 has a larger capacity of 5000 DWT (see Fig. 8). The basic specifications of the two vessels are listed in Table 1. Both are equipped with similar diesel engines, with a maximum speed of 900 r/min.

During the trials, main engine power and fuel consumption were recorded as the engine load increased from 50 % to full load. Fuel consumption measurements were taken at 50 %, 75 %, 90 %, and 100 % load conditions, and the consumption rate was determined based on the average of these measurements.

3.1.2. Validation of the model based on field measurement

The energy performance model aims to provide fast and accurate predictions of power and fuel consumption. Using the vessel profile, resistance prediction is first validated based on ship dimensions. Based on this, the propeller design and modelling are conducted using

(a) Vessel 1 (b) Vessel 2

Fig. 8. Images of the target vessels.

Table 1
Profiles of the two inland chemical tankers.

	Vessel 1	Vessel 2
Length overall [m]	99.60	105.04
Beam [m]	16.20	16.20
Draught [m]	4.40	4.80
Displacement [t]	3000	5000
Speed (100 % MCR) [kn]	12.05	11.04
Propeller diameter [m]	2.5	2.7
Number of propellers [−]	2	2
Engine power [kW]	2x662	2x648
Engine speed [rpm]	900	900

conventional blade profiles. The engine model is then established to predict power demand. Figs. 9 and 10 present the power prediction with validation against the actual measurement of Vessel 1 and Vessel 2, respectively.

The power prediction results indicate that the energy performance model captures the speed-power relationship of the two studied vessels effectively. The predicted fuel consumption rates are shown in Fig. 11, where good agreement with the measurements is observed, particularly around 90 % engine load. A positive sign indicates the percentage of overestimation compared to measurements, while a negative value indicates underestimation.

The model overestimates fuel consumption at lower engine loads because the predicted power is higher (see Figs. 9 and 10). Conversely,

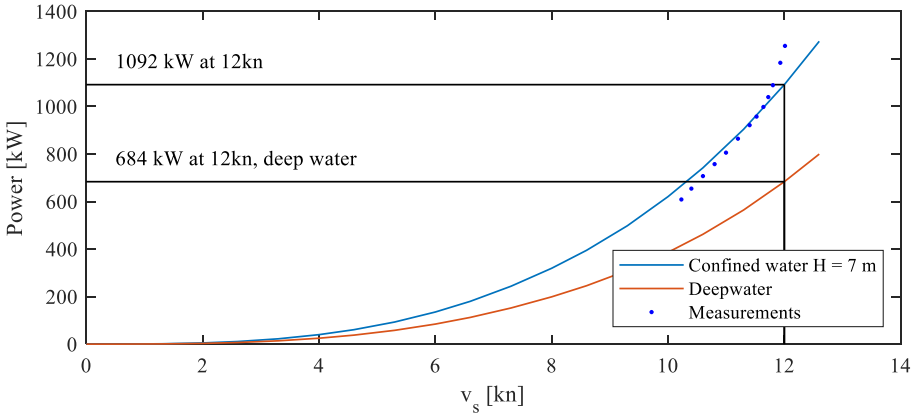

Fig. 9. Power prediction of Vessel 1 at $H = 7$ m.

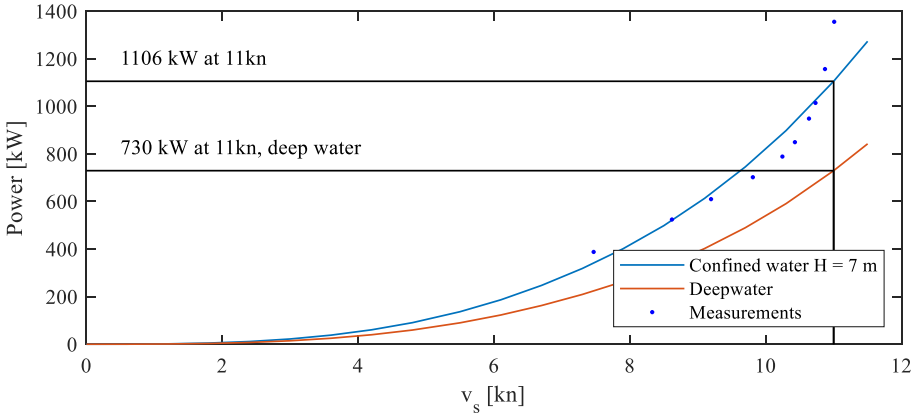

Fig. 10. Power prediction of Vessel 2 at $H = 7$ m.

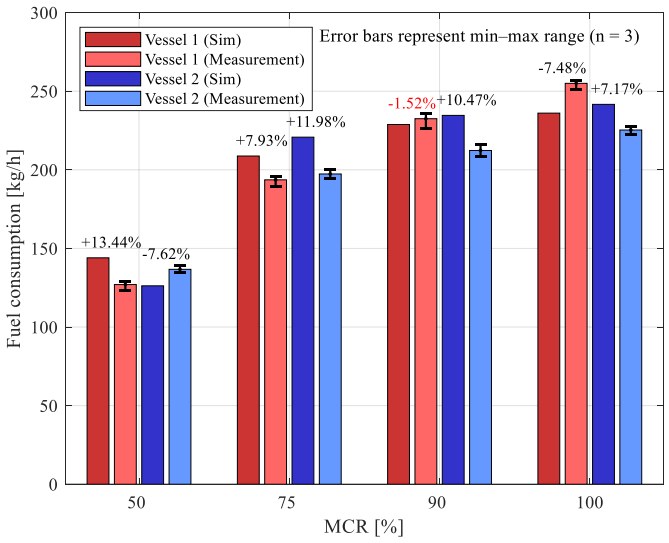

Fig. 11. Comparison between simulated and measured fuel consumption rates.

simulation results become slightly lower than the measurements (highlighted in red text) when the vessels approach fully loaded conditions. Across all loading conditions, the mean absolute error (MAE) of the fuel consumption prediction for the two vessels is approximately 8.45 %.

Since the model is based purely on empirical and analytical methods, and the input data include only the average water depth rather than detailed bathymetric information, the achieved accuracy—within a deviation of 10 %—is considered promising, especially given that only basic inputs (such as vessel and propeller dimensions, operational speed and water depth) are required.

Based on these results, it can be concluded that the energy performance model provides reliable predictions of power and fuel consumption, particularly considering the minimal input requirements.

3.2. Hydraulics modelling and simulation

This section presents the prediction results of the hydraulic model using bathymetry data from field measurements. The aim is to evaluate the accuracy of the riverbed modelling and the representation of cross-sectional shifts.

3.2.1. Cross-sectional shift prediction and validation

It is important to ensure that the proposed hydrological formula can accurately capture the cross-sectional shift in river meanders. To validate this, the formula is compared against field measurements taken at the confluence of the Wabash and Embarras Rivers in the United States [13]. Multibeam bathymetry data are shown in Fig. 12, with cross-section 4 selected as an example for maximum depth shift analysis. This cross-section is located roughly in the middle of the river bend, where a notable shift in the depth profile towards the outer bank is observed. Therefore, the skewness factor in Eq. (7) is assumed to be 1. The remaining parameters are the maximum cross-sectional water depth H_{MAX}, which is found to be 12 m, and the channel width 2b, which is approximately 140 m. Fig. 12 shows a width of 125 m, as the sonar measurements do not fully capture the river from bank to bank, which also explains why the measured depth is not starts at 0 m.

The cross-section can be predicted based on these parameters, and the result is shown in Fig. 13. The results demonstrate that the proposed equation accurately captures the trend of cross-sectional shifting. The location of the maximum water depth aligns well with the measurements. Deviations, particularly on the inner (left) bank, highlight the challenges of accurately predicting the riverbed slope deformation, which involves complex hydrodynamics and sediment transport processes. The primary objective of this formula is to offer a fast and efficient method for representing the general shifting of cross-sections in river meanders, which is achieved by correctly predicting the location of the maximum depth. Notably, as shown in Fig. 13, a distance of 20 m from the riverbank is already considered relatively close for vessel navigation; within this typical operational range, the model performs well in capturing the bathymetric profile.

3.2.2. River segment generation

To generate arbitrarily shaped river sections, this study uses a combination of straight and curved segments [39,63]. These segments are randomly generated within the initial ranges listed in Table 2. As discussed in Section 2.4.1, the river maintains a constant width, with 15 evenly distributed grid points in the lateral (cross-sectional) direction. In straight segments, the grid remains uniformly square-shaped, while in curved segments, the grids require longitudinal scaling based on the arc length at different lateral positions. Each new segment is transformed according to the position and orientation of the previous segment to ensure proper connectivity. At each cross-section, the bathymetry is generated using the hydraulic model, including cross-sectional shifts in

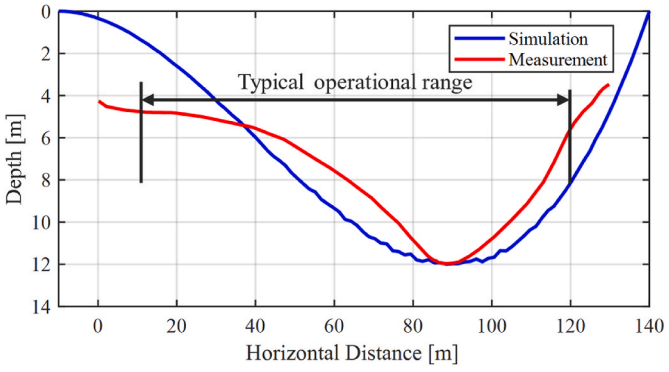

Fig. 13. Bathymetry modelling of cross-section 4 compared with measurements.

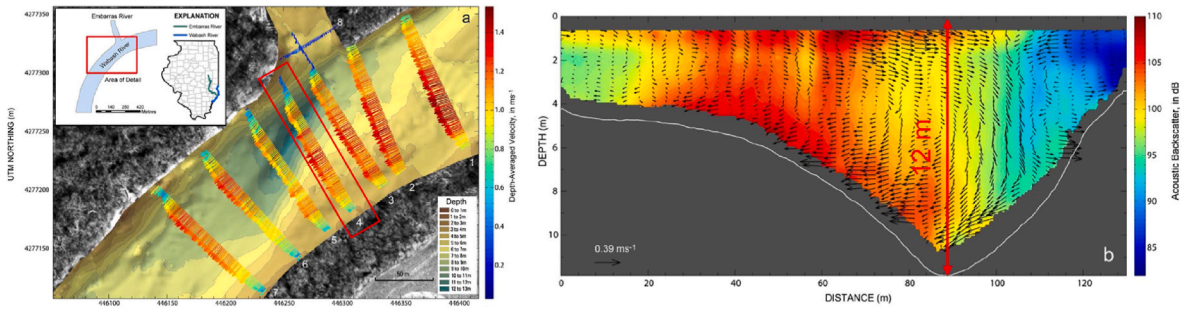

Fig. 12. Bathymetry and current measurements at the confluence of the Wabash and Embarras Rivers in the United States, reproduced from Parsons et al. [13].

Table 2
Initialisation parameters for river generation.

Parameter	Unit	Value
Length of straight segments	[m]	300–600
Radius of curved segments	[m]	300–500
Angle of curved segments	[deg]	30–90
Maximum river depth	[m]	10
Maximum current velocity	[m/s]	1.2
Grid resolution	[m]	15
Number of grids per cross-section	[−]	15

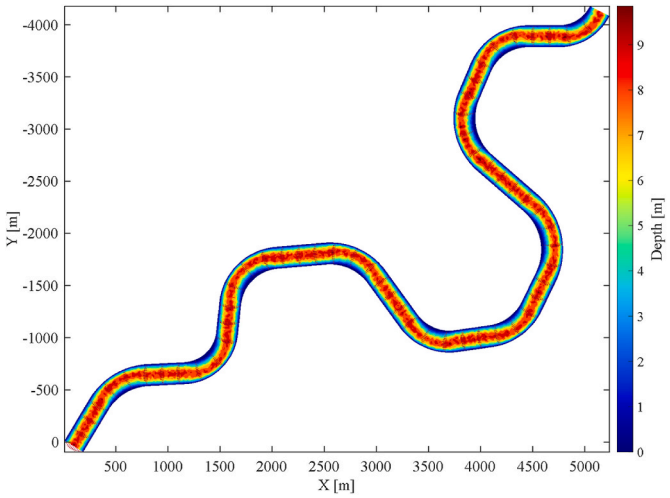

Fig. 14. Example A: 10-km-long waterway consisting of 20 segments.

curved segments.

Figs. 14 and 15 present two examples of generated river segments. Example A shows an approximately 10 km long waterway consisting of 20 segments, while Example B presents a longer waterway with 30 segments and a total length of 15 km. In the depth profiles, it is evident that the deepwater regions shift significantly towards the outer banks at sharper bends. Compared to straight segments with steady bathymetry distributions, vessel steering behaviour at bends—especially when navigating close to the inner banks—must be carefully examined, as shallow water and bank effects intensify with increasing confinement. In addition to navigational safety concerns, confined waters also lead to increased resistance and power demand, resulting in higher energy consumption.

In the following sections, systematic simulation and operational analyses are conducted using the two example waterways. The VPF is tested in various operational scenarios to demonstrate its capabilities in control implementation, path following, energy consumption prediction, and optimisation.

4. Operational analysis

This section presents simulation results under various scenarios, including sailing along the river centreline, path-following control near river infrastructure, and near-bank operations. The vessel's operational conditions are systematically analysed in terms of safety and energy efficiency. Path-following performance is evaluated using tracking errors and rudder actuation. By recording the vessel's state and dynamic power, the total fuel consumption for different routes can be assessed. Vessel A is selected as the reference ship, with a 70 % loading condition (2100 DWT) is initialised for shallow water conditions. Under this loading condition, the hydrodynamic derivatives are adopted from Koh and Yasukawa [65], as the ship used in their study has a similar overall length and displacement.

4.1. River centre navigation

Navigation along the river centreline is a typical operational mode for inland vessels when traffic conditions permit, as it helps avoid shallow water impacts and reduces the risk of grounding. Particularly in fully confined waters, operating near the centre also mitigates the hydrodynamic effects of riverbanks. In this scenario, the vessel maintains a constant propeller speed of 250 rpm to follow the upstream path along the waterway centre, using a waypoint resolution of 15 m. The control design is evaluated based on the trajectory, course offset (cross-track errors), and rudder actuation. A classical PID controller is used as a reference, with a sample period of 1 s. For a fair comparison, all control parameters are kept identical (see Table 3). The equations of motion are integrated using an explicit Euler method with a fixed simulation timestep of 1 s, which also matches the controller update rate. The resulting trajectories from the two rudder control methods are shown in Fig. 16.

It is important to note that the incremental PID outperforms the conventional PID controller by maintaining smaller deviations from the target trajectory. The quantitative cross-track error (XTE) is presented in Fig. 17, and it can be seen that the incremental PID effectively reduce the course offset with lower XTE.

In addition to tracking performance, the control efforts (rudder

Table 3
Parameterisation of the controller settings.

Controller	Parameter	Value
PID	K_p	1.5
	T_i	50
	T_d	15
Incremental PID	K_p	1.5
	T_i	50
	T_d	15
	T_s	1

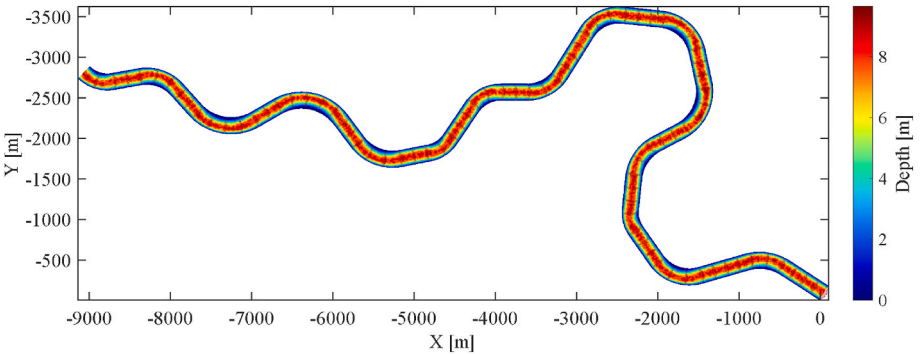

Fig. 15. Example B: 15-km-long waterway consisting of 30 segments.

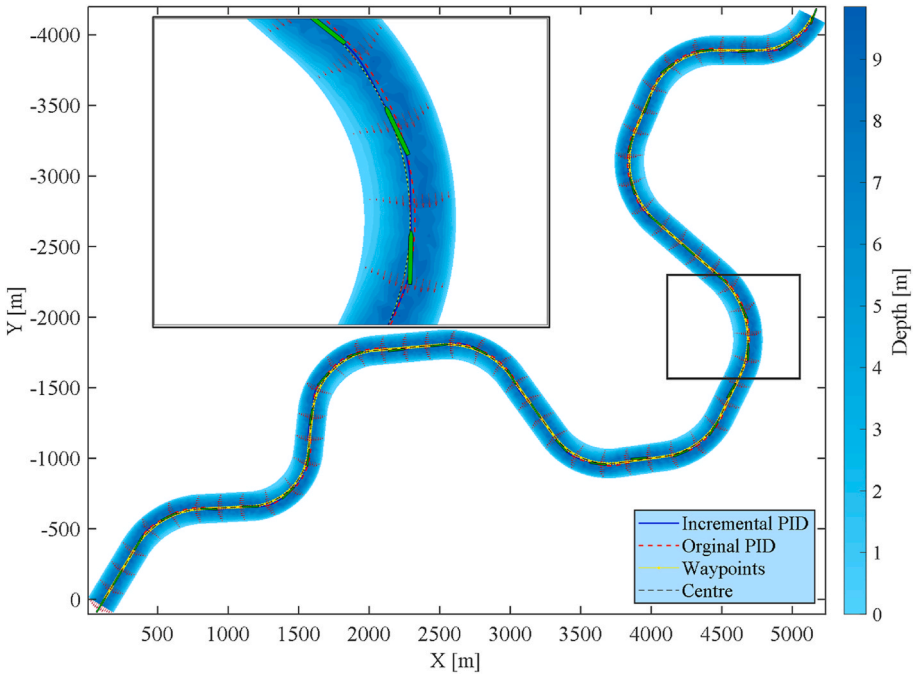

Fig. 16. Vessel trajectories during river centre navigation, red for original PID, blue for incremental PID.

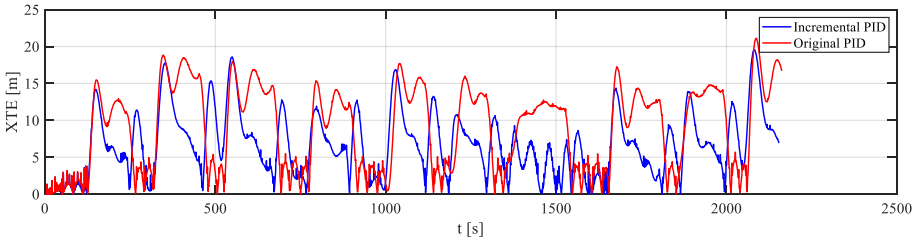

Fig. 17. Time histories of the absolute cross-track error (XTE).

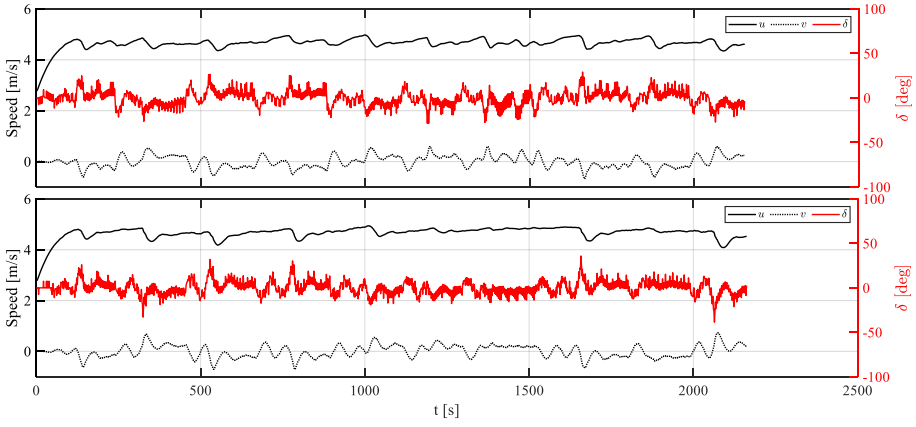

Fig. 18. Vessel speed and rudder actuation: Incremental PID (top) and original PID (bottom).

actuation) are evaluated in Fig. 18, where the classical PID shows more frequent oscillations and higher rudder peaks, particularly in curved segments of the route. This reflects a key limitation of purely state-based controllers under nonlinear and time-varying conditions: the vessel requires more frequent rudder adjustments to follow a dynamically changing path in confined waters. In contrast, the incremental PID improves robustness and control stability by suppressing cumulative errors and limiting abrupt actuation, making it more suitable for such scenarios. Given these advantages, the incremental PID will be used in the following sections.

4.2. Navigation near infrastructure

In inland waterways, the presence of various artificial structures, such as bridges and locks, necessitates careful consideration of manoeuvring and control design. These structures further constrain the

available operational space. Bridges and locks serve essential operational functions, where bridges impose lateral clearance constraints that require cautious speed control for safe passage, while locks regulate water levels and require vessels to come to the chamber with a complete stop. The simulation presented in this subsection evaluates the performance of the VPF when the vessel encounters bridge pillars and locks. The vessel maintains a constant propulsion speed until it approaches a bridge pillar or lock. When approaching these structures, the propeller speed must be reduced, and if necessary, reversed to bring the vessel to a stop. The range is determined by the distance ahead (S_d) between the vessel's current position and the structure, as expressed by:

$$n = \begin{cases} 0.5n_{max}, & S_d \ll 2L(pass\ bridge) \\ -0.5n_{max}, & S_d \ll 3L(stop\ at\ lock) \end{cases} \tag{11}$$

When the ship approaches a bridge within a distance of less than twice the ship's length, the propeller load is reduced to 50 % to ensure safe passage. Additionally, the propeller must rotate astern to stop the ship when nearing river locks. The river map, along with the bridge, lock, and resulting vessel trajectory, is presented in Fig. 19. The route is shifted to maintain a constant lateral distance of 2 grids (30 m) from the waterway centreline, where the vessel maintains the same 250 rpm as in the previous section to follow the route. The vessel speed is adjusted based on the distance (S_d) to the bridge and lock infrastructure. The bridge is located at the centre of the river segment, which has an overall length of 210 m, matching the channel width. The span between each bridge pier is 30 m. The river lock, situated at the upper right part of the map, is divided into two chambers, designed to facilitate double-lane vessel passage.

From the results shown in Fig. 19, it can be concluded that the vessel successfully follows the desired route, even under disturbances caused by the riverbank and infrastructure. The bottom bounding box highlights the vessel's ability to pass through the bridge safely with reduced RPM. The heading angle aligns well with the route, and no significant drifting is observed during this manoeuvre. It should be noted that the hydrodynamic impact from the bridge pillars is neglected here. Studies such as Du et al. [66] have conducted CFD and experimental analyses to evaluate the impact of bridge piers on passing vessels in confined waterways, with the most significant effect observed in the longitudinal direction (resistance). Since the vessel typically operates at the centre between two bridge piers, and their size is relatively small compared to the vessel. Hence, the lateral impact is minor compared to the normal bank effect. Therefore, from a manoeuvring perspective, this paper does not consider the hydrodynamic effects of the bridge piers on vessel handling, especially the influence of lateral forces and moments. In contrast, the lock has a significant size and obvious constraints, where the bank effect cannot be neglected.

When the vessel approaches the lock, the propeller starts to rotate astern, effectively stopping the vessel within the lock chamber, as indicated by the top bounding box. It should be noted that when the vessel enters the lock chamber, rudder control is disabled once the speed falls below a certain threshold, as the reversing propeller continuously decelerates the vessel, and the rudder becomes ineffective at such low speeds. At this stage, the primary objective is no longer course-keeping but rather bringing the vessel to a complete stop within the lock. From the trajectory, since there is no rudder control, some pure bank effect from a channel wall can also be noticed, with the vessel showing an obvious bow-out movement. Fig. 20 presents the variation in vessel speed based on rudder actions. The vessel maintains a relatively constant speed for most of the time, undergoing an obvious speed drop when it is close to the bridge and fully stops at the end when it approaches the lock. The rudder control remains deactivated when the vessel speed is less than 2 m/s during deceleration. In addition, it should be noted that the vessel is considered entirely stopped when its speed drops below 0.1 m/s.

4.3. Near-bank operation

The third typical operational condition is near-bank sailing, as inland vessels often need to sail close to one side of the bank to ensure safe passing between oncoming or overtaking vessels. In these situations, the vessel's steering must be carefully examined, as a closer distance to the bank induces stronger hydrodynamic forces on the vessel. Due to the asymmetry of bathymetry in river bends, sailing near inner banks can result in a significantly stronger shallow water effect, affecting both navigation safety and energy efficiency.

In this section, River B is selected as the operating waterway. The

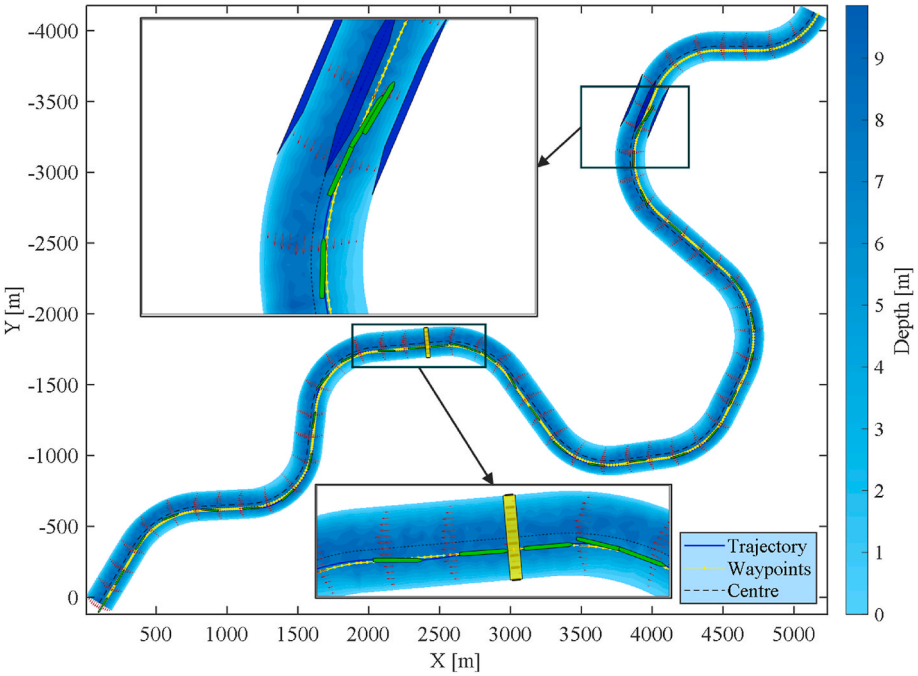

Fig. 19. Simulation of vessel operations near infrastructure, including a bridge and lock.

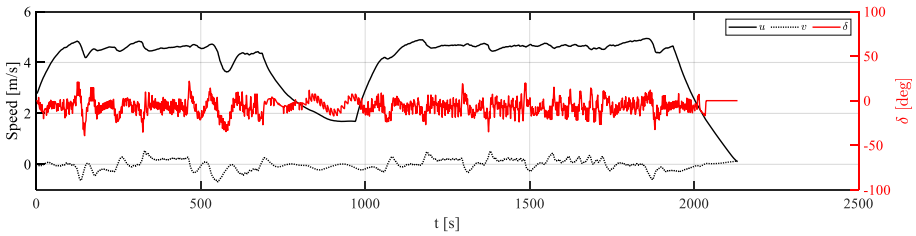

Fig. 20. Time histories of ship surge (u) and sway (v) speeds with rudder actuation.

simulation is conducted at various ship-bank distances to assess the vessel's handling performance under increasing hydrodynamic disturbances. In addition, an energy analysis is carried out to study the impacts of these disturbances on fuel consumption. Fig. 21 shows the trajectory along a predefined route close to the right bank. The route maintains a constant distance of 30 m from the bank, where the nondimensional ship-bank distance y_B' is 0.214, calculated using the equation below:

$$y_B' = y_B / W_C \tag{12}$$

where y_B is the ship-bank distance in metres, and W_C is the channel width. Thus, $y_B' = 0.5$ indicates the vessel sails at the waterway centreline. During route initialisation, the depth data are checked at each waypoint, and necessary modifications are made to ensure the depth is deeper than the ship's draught for safe passage.

In general, the results show that the vessel can successfully follow the target route on this complex waterway. The incremental PID controller in this study shows practical advantages for path following in confined water. Its simplicity and low computational cost make it particularly suitable for real-time applications onboard systems. However, compared to more advanced control methods such as MPC and reinforcement learning-based control, incremental PID lacks the ability to explicitly handle system constraints or anticipate future disturbances based on model predictions. For instance, when it approaches the inner bank with decreasing water depth, as shown in the zoomed-in sub-figures, significant bank effects are observed at certain bends, causing course deviations. This is further compared with a near-centre sailing condition, as shown in Fig. 22, where the left figure shows results under minor bank effects. The trajectories demonstrate that the vessel struggles to follow the path when operating close to the banks. The results underscore the significant impact of external disturbances on vessel navigation in confined waterways, emphasising the need to account for these physical effects in onboard navigation system design. In future works, the control scheme will be improved through more proactive approaches, e.g. taking the vessel turning advanced distances into account to consider the actual vessel reaction times. In addition, adaptive control schemes [67] can be employed to further improve the robustness of the vessel controller under highly confined water.

The impact of confined water at these curves is further illustrated in the speed and power plots shown in Figs. 23 and 24, respectively. As the vessel approaches the inner bank and the water depth decreases, it experiences noticeable speed reductions, as highlighted in Fig. 23. In addition to increased shallow water resistance, the reduced under-keel clearance introduces additional bank-induced force and moments, leading to vessel drift and course deviation. Consequently, the required brake horsepower P_{BH} also increases in these critical regions, as indicated in Fig. 24. With dynamic power predictions, the total energy consumption can be calculated based on the vessel's speed and sailing time.

The results of tracking performance (XTE) and fuel consumption at varying y_B' values under different water current directions are presented in Table 4, where the maximum current speed is approximately 1.2 m/s. The influence of water current on sailing time is most significant when navigating near the river centre, where the flow velocity is highest. Consequently, the speed difference between upstream and downstream navigation becomes more pronounced, with time differences exceeding 700 s when $y_B' = 0.428$.

Regarding tracking performance, in upstream operation, the tracking errors remain relatively small, although a certain course offset can be observed when the vessel approaches the bank. In contrast, during downstream operation, the rudder steering force is reduced due to the lower relative inflow velocity. As a result, vessels experience larger XTEs as the vessel approaches the shallower near-bank region.

In terms of energy consumption, the most significant factor remains the water current, which directly affects the estimated time of arrival

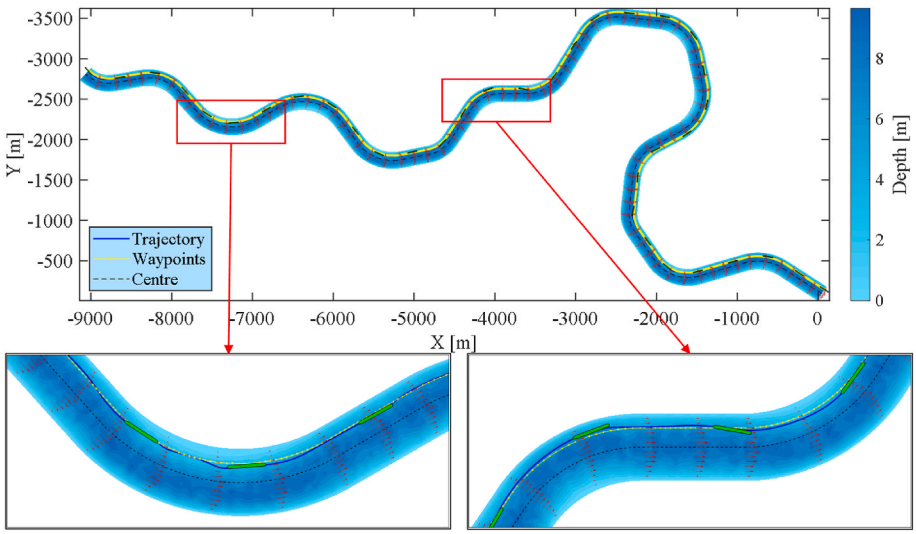

Fig. 21. Vessel trajectory during near-bank navigation. The initial ship-bank distance is 30 m, corresponding to $y_B' = 0.214$.

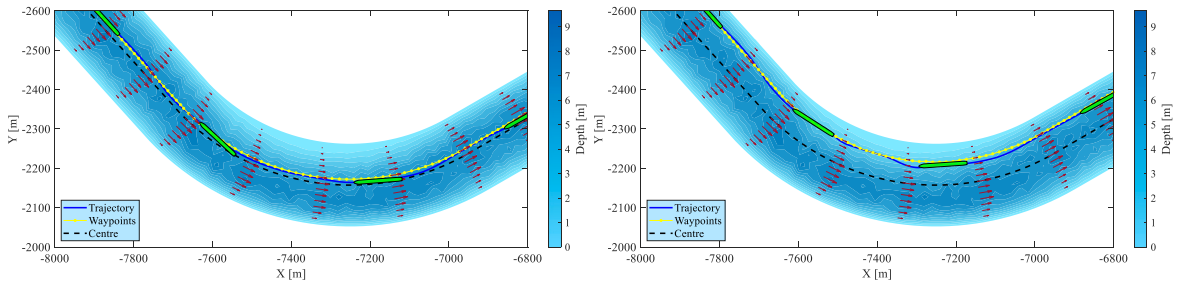

Fig. 22. Vessel trajectories under two different ship-bank distances.

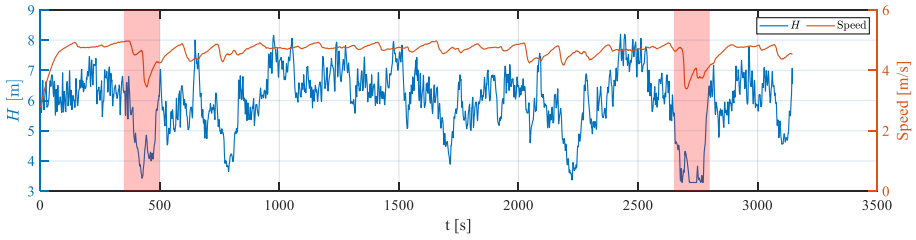

Fig. 23. Variation of ship speed with corresponding water depth, $y'_B = 0.214$.

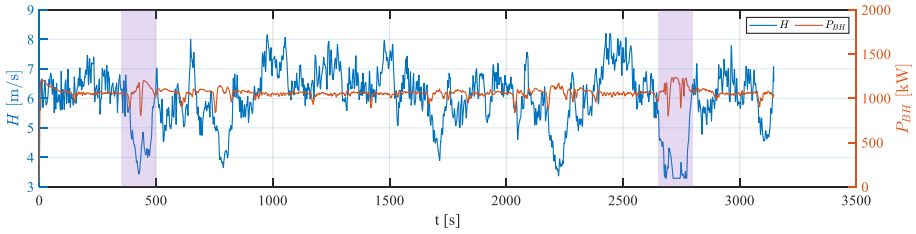

Fig. 24. Shallow water effect on dynamic brake horsepower (P_{BH}), $y'_B = 0.214$.

(ETA). Fuel consumption under upstream conditions is 25 % higher than in downstream conditions. It is also evident that decreasing ship-bank distances introduce additional energy costs due to increased hydrodynamic effects. For both current directions, a lower y'_B value results in higher energy consumption.

This trend is further illustrated in the variations of ship speed and power shown in Figs. 25 and 26. As the vessel sails closer to the bank, it experiences a noticeable reduction in surge (longitudinal) speed due to decreasing water depth. In addition, the increased side forces and moments induce greater sway motion, particularly at smaller y'_B, increasing the drift angle. This leads to greater course deviations (as shown in Fig. 22) and higher energy demand, as more power is required to maintain the heading in oblique flow conditions, as illustrated in Fig. 26.

The result indicates that, although the vessel operates at a relatively ideal constant RPM (80 %), significant increases in power demand and energy consumption are still observed due to course deviations caused by strong shallow water and bank effects during near-bank navigation in river bends.

Overall, the simulations under various scenarios demonstrate the capability of the proposed VPF to capture the vessel's operational performance. The results show that the proposed VPF can serve as a rapid and effective platform for a range of purposes, including testing control strategies, evaluating operational performance, and assessing energy efficiency across a wide range of inland waterway conditions.

However, it should be noted that the manoeuvring simulations require further validation against full-scale trial data. In this study, the studied vessel adopts hydrodynamic derivatives from a pusher-barge model with similar length and displacement, as no validated hydrodynamic data are available for this specific vessel. While the global dimensions are comparable, the hull forms are not similar, which may result in differences in manoeuvrability for the actual ship dynamics (e.g., gap flow interactions in the pusher-barge configuration). This limitation should be addressed in future work through systematic CFD simulations to derive vessel-specific hydrodynamic coefficients for the target vessel.

5. Energy optimisation

Optimising energy consumption is crucial for future autonomous inland vessels to enhance transport efficiency. By optimally tuning vessel speed according to the sailing environment, the intelligent onboard system can improve operational resilience and support sustainable waterborne transport with lower emissions.

Table 4
Fuel consumption at varying ship-bank distances y'_B under upstream and downstream currents.

y'_B [−]	Current direction [−]	Distance travelled [km]	Sailing time [s]	Maximum XTE [m]	Fuel consumption [kg]
0.214	Upstream	14.573	3146	17.40	200.8
	Downstream	14.594	2561	27.20	164.8
0.285	Upstream	14.574	3103	17.17	193.5
	Downstream	14.638	2554	24.55	162.9
0.428	Upstream	14.590	3110	16.26	189.6
	Downstream	14.626	2398	20.05	149.7

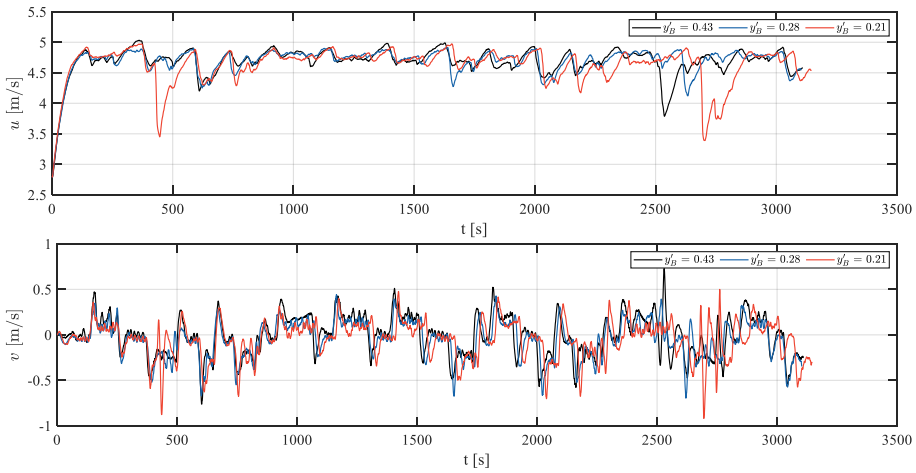

Fig. 25. Vessel surge and sway speeds (u, v) over ground for upstream navigation under varying ship-bank distances.

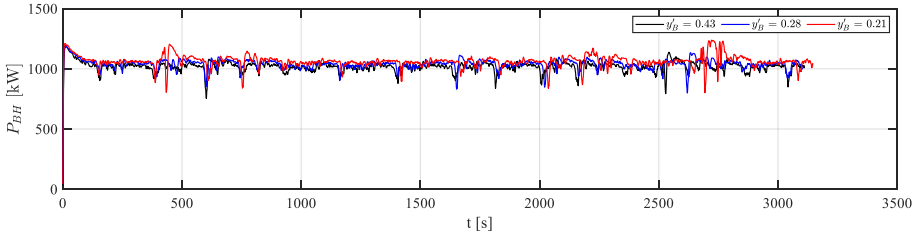

Fig. 26. Time histories of P_{BH} for upstream navigation under varying ship-bank distances.

This section presents the procedure and results of energy optimisation for autonomous vessels. The aim is to optimise speed settings along a fixed route to minimise energy consumption while ensuring the ETA meets time requirements. As discussed in previous sections, shallow water has significant impacts on propulsion power and energy costs. Therefore, the focus here is to use an optimisation algorithm to adjust vessel speed appropriately based on the encountered waterway profiles—namely, water depth and bank distance.

The schematics of the speed optimisation are shown in Fig. 27. A target route of 10 km is divided into several segments by waypoints. These waypoints are projected into the solution space of the optimisation problem, incorporating individual factors that affect fuel consumption, such as water depth, ship-bank distance, and current profile. With ship speed as a variable and the engine model incorporated, the fuel cost function at each leg (FC_{leg}) is established. The role of the PSO algorithm is to adjust the ship speed to (a) minimise total energy

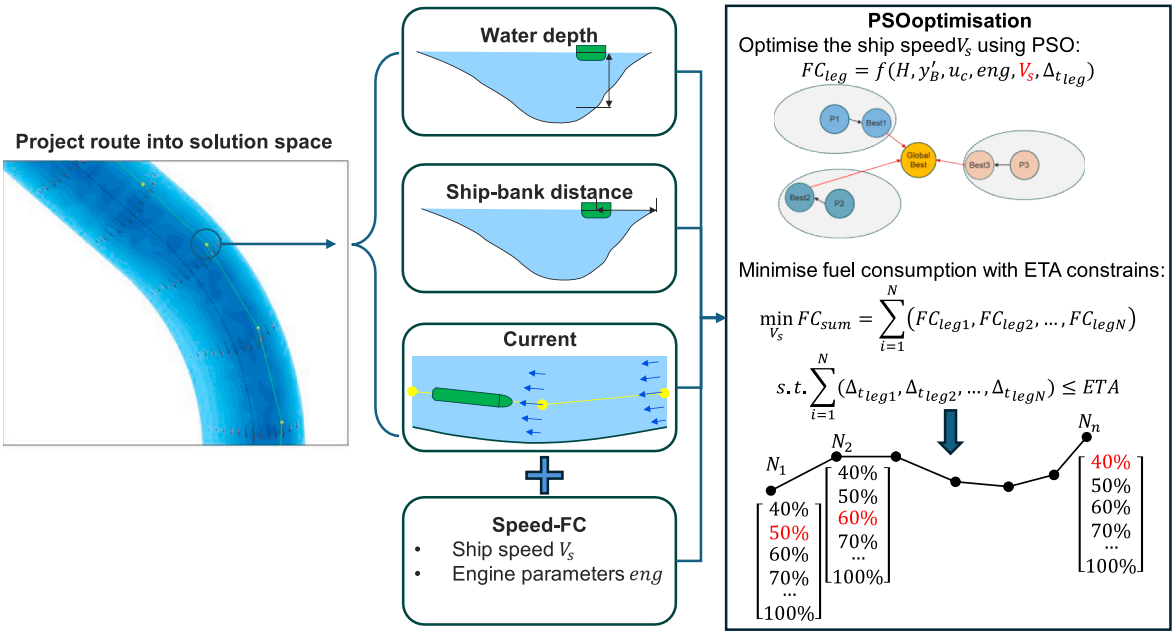

Fig. 27. Schematics of vessel speed optimisation for reducing fuel consumption.

consumption (FC_{sum}) over the entire route, and (b) ensure total sailing time satisfies the ETA constraints. The required ETA is calculated based on a fixed reference ship speed.

5.1. Impact of initial values

An essential feature of swarm-based algorithms is that their effectiveness and convergence speed rely significantly on the initial values. To quantify this impact on the performance of the PSO algorithm, a speed initialisation is conducted based on the corresponding water depth along the entire route. The selection of ship speed falls in the range of 60 %–90 % of the maximum speed V_{MAX}, and the speed is reduced according to an exponential function, given as:

$$V_i = \begin{cases} 0.6 \cdot V_{MAX} & (r_i \le 1.2) \\ 0.6 \cdot V_{MAX} \cdot \left(0.6 + 0.3 \cdot \left(1 - e^{-\alpha \cdot (r_i - 1.2)}\right)\right) & (1.2 < r_i \le 3.0) \\ 0.9 \cdot V_{MAX} & (r_i > 3) \end{cases} \tag{13}$$

where r_i is the depth-to-draft ratio at waypoint i ($r_i = H_i / T$), α is a factor controlling the rate of speed reduction with respect to water depth (assumed to be 1 in this study), and V_{MAX} is 7.45 m/s (14.5 knots).

To achieve a comparable ETA at the beginning, these initialised speed values are normalised to ensure their average equals the constant target speed (80 %), given as:

$$\begin{aligned} \overline{V} &= \frac{1}{N} \sum_{i=1}^{N} V_i \\ V_i' &= V_i \cdot \frac{0.8 \cdot V_{MAX}}{\overline{V}} \end{aligned} \tag{14}$$

where V_i' is the normalised initial speed at each waypoint. Based on this, the initial speed profile corresponding to the waterway bathymetry is shown in Fig. 28. The profile reflects the influence of water depth on vessel dynamics. The speed remains relatively constant in the deeper, central parts of the waterway where shallow water effects are minimal. However, in near-bank areas with predominantly shallow water, the speed is adjusted according to depth variations, thereby offering a physically consistent and reasonable initial value for the optimisation process.

The initial parameters of PSO keeps constant through all optimisations (see Appendix C). Fig. 29 shows the optimisation history of total fuel consumption along the route near the river centre and compares results with and without the speed initialisation method. The results indicate that the proposed speed initialisation based on water depth distribution effectively improves the performance of fuel optimisation. It can be seen that the algorithm generates populations with very high fuel costs when using random initial values. By contrast, applying the speed adjustment method yields noticeably lower fuel consumption from the first iteration. Overall, it can be concluded that compared with the random speed selection—which achieves a 2.05 % fuel reduction—the proposed speed initialisation method enables better convergence and results in a lower final fuel cost (2.77 % fuel savings) under the same iteration conditions.

5.2. Impact of shallow water

The optimisation study is conducted under two different ship-bank distances to investigate the potential for energy savings: (a) river centre navigation with $y_B' = 0.5$, and (b) near-bank sailing with $y_B' = 0.214$. Fig. 30 shows the results for upstream conditions. It can be observed that maintaining a fixed service speed near the shore noticeably increases fuel consumption compared to sailing in the relatively deep water at the river centre. Although the current speed is lower near the bank than at the centre, the shallow water effect remains dominant, resulting in approximately 6 % higher fuel consumption. This also suggests that under such conditions, the optimisation method has greater potential for reducing fuel use, as more shallow water regions near the bank make it beneficial to dynamically adjust the vessel speed to minimise resistance and energy consumption, as shown in Fig. 30(b).

In downstream conditions, as shown in Fig. 31, the differences in fuel consumption between the two ship-bank distances are more significant since the vessel sails at a higher speed over the ground. Regarding the performance of the PSO algorithm, it can be concluded that, compared with the upstream condition, a similar trend in fuel consumption reduction is observed, with more fuel saved when operating near shallow water regions. Detailed results from the fuel consumption optimisation are presented in Table 5. The PSO algorithm achieves fuel savings while ensuring that the ETA strictly complies with the time constraints along each route. In addition, the shallow water effect has a minor impact when the vessel sails at the waterway centre. However, an average fuel savings of 2.8 % can still be achieved using the PSO algorithm with the proposed speed initialisation method. Higher fuel savings are observed when the route is shifted closer to the bank, as both shallow water and channel banks introduce additional forces. Under this condition, a promising fuel savings of 5.8 % can be achieved through proper speed optimisation. These results highlight the importance of tuning the operational mode according to the encountered waterway conditions. For future autonomous inland vessels, particularly those equipped with fully electrified propulsion systems [68,69], the proposed energy optimisation methods can provide significant benefits by reducing bunkering frequency and enhancing operational duration.

Since this study considers only speed optimisation, the application is limited to conventional diesel engines. In future work, the optimisation problem will be extended to include joint rudder and speed

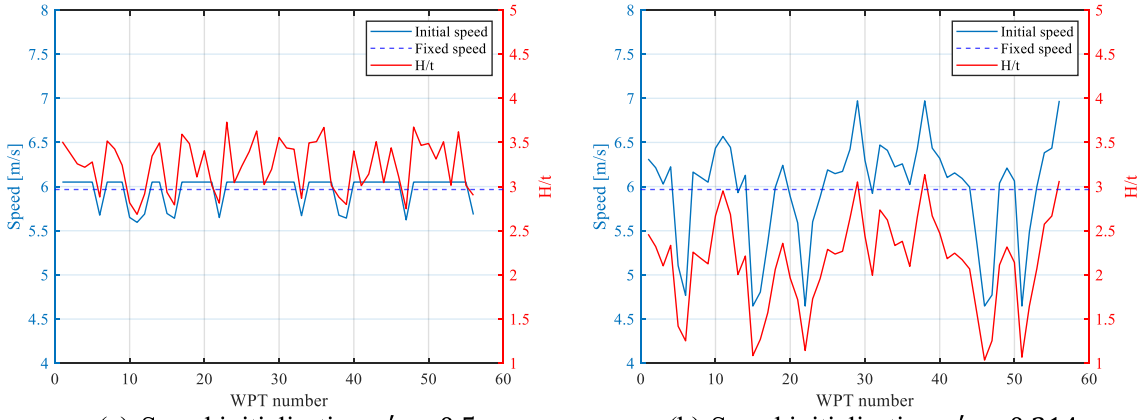

Fig. 28. Initial speed profile based on water depth along two target routes with different ship-bank distances.

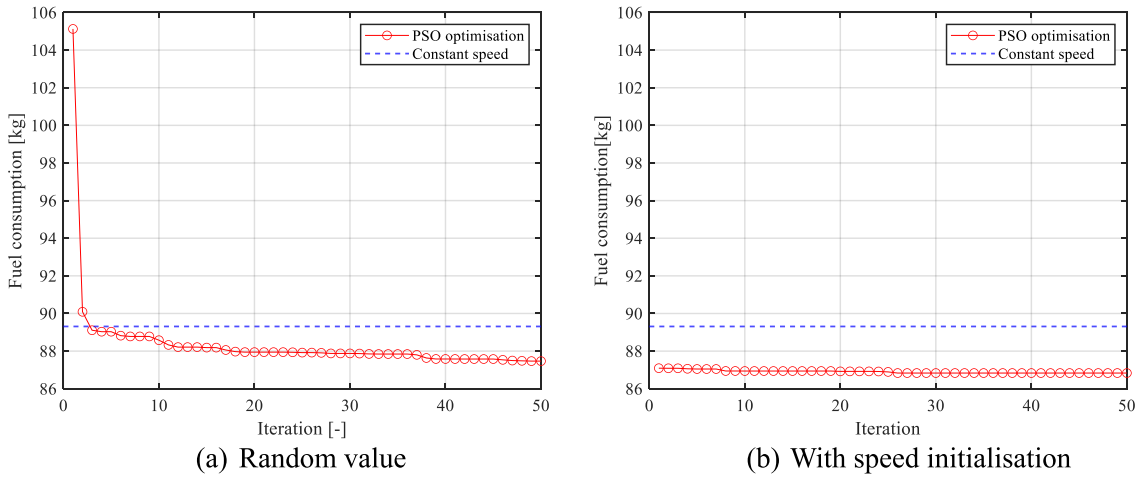

Fig. 29. Optimisation history of fuel consumption using PSO for a route near the river centre.

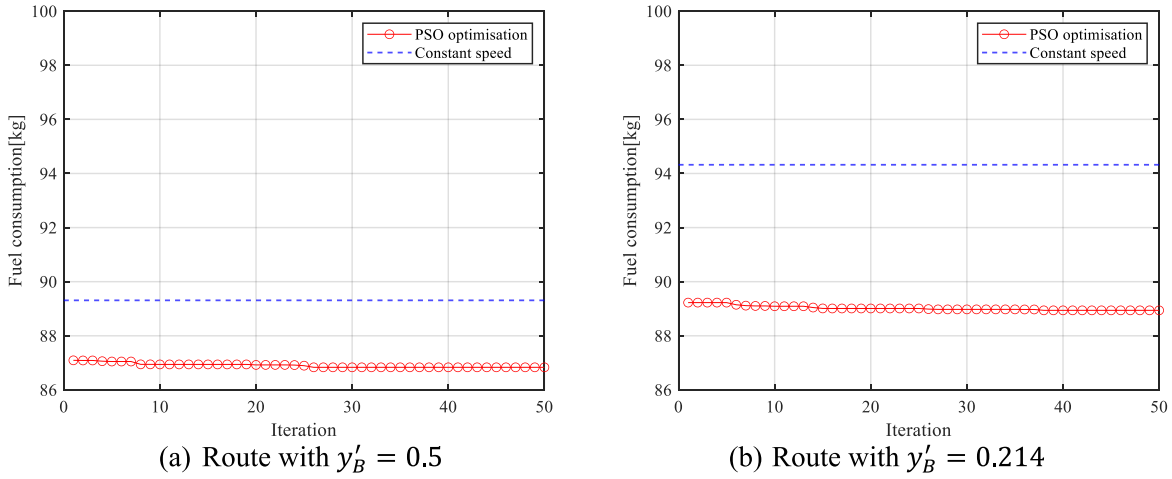

Fig. 30. Optimisation results under different ship-bank distances; current direction is upstream.

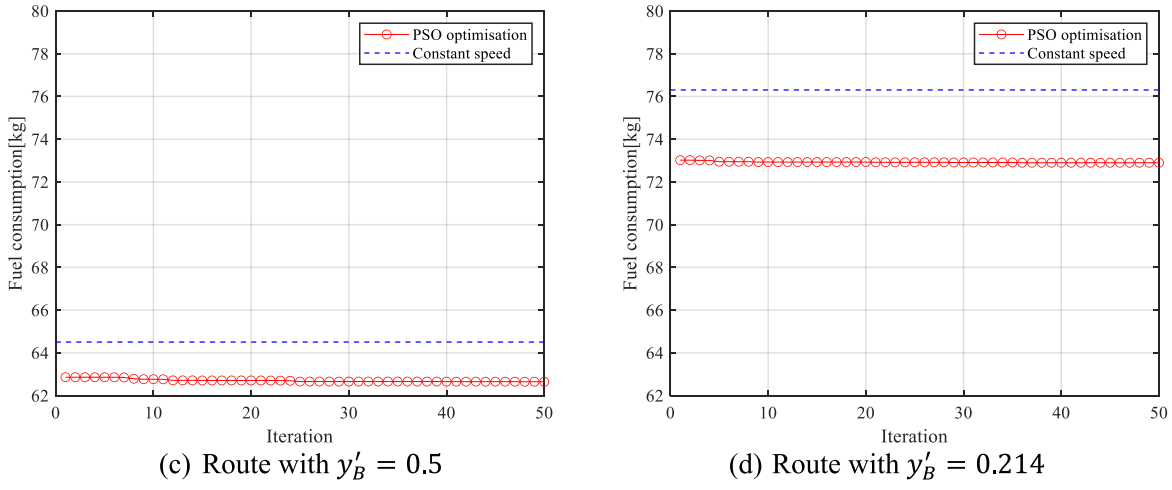

Fig. 31. Optimisation results under different ship-bank distances; current direction is downstream.

optimisation, as optimising rudder control can also help avoid unnecessary deflections and reduce energy consumption. This introduces a more complex optimisation challenge, as the solution space is expanded to include additional factors such as drift angle and rudder forces. Therefore, more advanced optimisation algorithms, such as those based on reinforcement learning, will be employed to enhance optimisation performance. In addition, a cost-effectiveness analysis will be conducted to compare different energy carriers—such as hybrid and fuel cell systems—which are crucial for autonomous and fossil-free shipping.

Table 5
Detailed results of energy optimisation under different ship-bank distances and current directions.

y_B' [−]	Operational mode [−]	Current [−]	ETA [s]	FC [kg]	Fuel savings [%]
0.5	Fix speed	Upstream	1938.30	89.29	–
	PSO optimisation	Upstream	1938.18	86.81	2.77
0.214	Fix speed	Upstream	1821.94	94.33	–
	PSO optimisation	Upstream	1821.52	88.87	5.78
0.5	Fix speed	Downstream	1399.98	64.50	–
	PSO optimisation	Downstream	1399.90	62.65	2.86
0.214	Fix speed	Downstream	1465.27	76.30	–
	PSO optimisation	Downstream	1465.25	72.89	4.47

6. Conclusions

Autonomous inland vessels are considered a competitive solution for enhancing the efficiency and sustainability of waterborne transport, contributing to lower emissions and reduced operational costs. In this context, this study focuses on designing a voyage planning framework, a key technology for monitoring and evaluating the operational energy performance of autonomous inland waterway vessels.

Existing studies on inland vessels tend to focus on specific aspects, such as hydrodynamics (e.g. CFD) or sophisticated control design. However, a comprehensive system for generic energy performance and operational analysis is missing. To address this gap, this study presents the design of a novel, holistic VPF for the energy prediction of autonomous inland vessels, including coupled effects between hydrodynamics and control. The modular structure of the VPF allows it to be adapted to other inland vessel designs, energy systems, and waterway types, making it a versatile tool for early-stage evaluation and onboard decision-making. The main contributions and findings can be summarised as follows.

(1) The framework establishes a physical environment that reflects the characteristics of inland waterways and, based on this, supports the design and energy performance prediction of autonomous inland vessels. It offers a comprehensive operational analysis through energy prediction under hydrodynamic and hydrological impacts, with detailed interactions from vessel manoeuvring and motion control.
(2) A new hydraulic model is proposed to simulate depth variations along river bends, enabling the analysis of how inland waterway topography affects vessel energy consumption and manoeuvrability. The proposed formula is validated using actual field measurements from a river in the U.S. The results demonstrate that the model can correctly capture the cross-sectional shift in river meanders, providing physics-based waterway conditions for vessel operational analysis.
(3) A systematic vessel operational analysis has been conducted under various route and environmental conditions to showcase the VPF's capability in evaluating the safety and energy efficiency of AIWVs. The simulation includes various typical conditions, such as waterway centre navigation, bridge passage and stopping near waterway locks, near-bank sailing, and energy analysis. The results indicate that the presence of shallow water and channel banks leads to significant disturbances in vessel energy consumption and steering. Apparent vessel course deviations and additional fuel consumption are observed when the ship-bank distance is less than 25 % of the channel width.
(4) An energy optimisation method based on a PSO algorithm was proposed. A water depth-based vessel speed initialisation technique was introduced, showing significant improvements in fuel consumption reduction and convergence performance. It is concluded that using proper vessel speed optimisation methods, fuel savings of up to 5.8 % can be achieved in near-bank shallow water regions, while in deeper areas near the channel centre, the savings decrease but still average around 2.8 %.

While the proposed VPF integrates key models for inland navigation, its application may be limited by the availability of high-resolution bathymetry or flow data for real-world onboard applications. To address this, sensor fusion techniques could be adopted to improve robustness under incomplete or uncertain input conditions.

In future work, the framework will be enhanced in the following areas: (a) enhancing the energy performance model to include other energy carriers, such as fuel cells and batteries, especially for electrified vessels; (b) improving optimisation techniques through online approaches, e.g. using deep reinforcement learning to dynamically adjust speed and rudder to minimise energy consumption and control efforts; (c) exploring model-based control methods, such as model predictive control (MPC), particularly by accounting for environmental disturbances (e.g., wind, current) either as bounded uncertainties or probabilistic inputs. Data-driven MPC will also be investigated as a promising approach to better capture vessel dynamics and enhance control performance; (d) enhancing vessel dynamics modelling by conducting dedicated CFD-based manoeuvring simulations and establishing a hydrodynamic derivative database for various vessel types to broaden the framework's applicability.

CRediT authorship contribution statement

Chengqian Zhang: Writing – review & editing, Writing – original draft, Validation, Methodology, Investigation, Formal analysis, Conceptualization. **Chi Zhang:** Writing – original draft, Methodology, Investigation, Conceptualization. **Fabian Thies:** Writing – review & editing, Validation, Supervision. **Wengang Mao:** Writing – review & editing, Supervision, Project administration, Funding acquisition. **Jonas W. Ringsberg:** Writing – review & editing, Writing – original draft, Supervision, Project administration, Methodology, Funding acquisition.

Declaration of competing interest

The authors declare that they have no known competing financial interests or personal relationships that could have appeared to influence the work reported in this paper.

Acknowledgements

This work has received funding from the European Union's Horizon 2020 research and innovation programme under the Marie Skłodowska-Curie Grant Agreement No. 955768 (ETN AUTOBarge). For more information, please visit the project website: https://etn-autobarge.eu/.

Appendix A. Ship energy performance modelling

The energy systems of the two inland chemical tankers in Section 3 are modelled using the ship performance model ShipCELAN-IWV Zhang et al. [10], which is designed specifically for inland vessels. The ship's shallow water resistance is predicted using the equation below:

$$R_T = 0.5\rho_{FW} {V_S}^2 S_W C_T + R_S + R_{BANK} \tag{A.1}$$

where ρ_{FW} is the freshwater density, V_S represents the ship's speed, S_W is the wetted surface area, R_S is the additional resistance due to squatting in shallow water, R_{BANK} represents the resistance due to the bank effect, and C_T is the total resistance coefficient. The total resistance coefficient is computed as:

$$C_T = \left(1 + \left(k_{deep} + \triangle k\right)\right) C_F^* + C_W \tag{A.2}$$

where k_{deep} represents the form factor in deep water, Δ_k is the correction on the form factor in shallow water from Millward [70], and C_F^* is the frictional resistance, including the shallow water effect [5].

In Eq. (A.1), the resistance due to squat is calculated using the equation:

$$R_S \Big/ R_T = \left(\Delta_{sinkage} A_{WP} / \nabla\right)^{2/3} \tag{A.3}$$

where $\Delta_{sinkage}$ is the sinkage in shallow water, ∇ is the ship displacement in (m3), $\Delta_{sinkage}$ is taken from a prediction method based on ship fullness and depth Froude Number (Fr_h) [4]. The other term, bank-induced resistance (R_{BANK}) in Eq. (A.1) is derived using the regression curve in ShipCELAN-IWV. The model can be found from Zhang et al. [10] in detail.

Based on the shallow water resistance prediction, the propeller is designed using OpenProp [71], according to the basic propeller dimensions and the ship's service speed. Figure A. 1 shows an example of the propeller geometry of vessel 2, and the corresponding open water efficiency curve is presented in Figure A. 2.

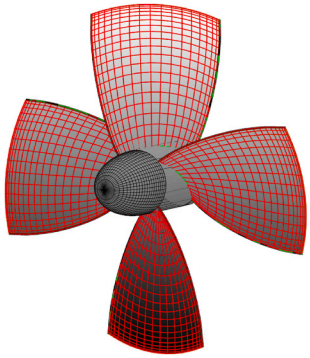

Fig. A. 1. Propeller geometry of Vessel 2 in Section 3, where the two vessels have similar propellers.

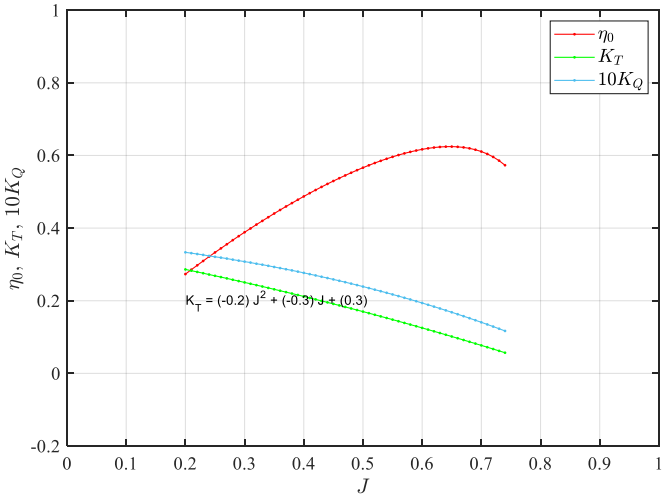

Fig. A. 2. Propeller open-water efficiency curve of Vessel 2.

The prediction of the engine *SFOC* was taken from the regression model in Ref. [56]. The model was built on measurements from various marine engine manufacturers, e.g., Cummins, MAN, Caterpillar, and Wärtsilä, with different power ranges. The detailed model is presented in Table. A. 1

Table. A. 1
Regression model for the engine *SFOC* prediction.

P_{max} [kW]	$X = P_S/P_{max}$ [%]	$SFOC = f(X)$ [g/kW/h]	Error [%]
100–300	0–20	$398.89X^{-0.1987} + 8.945$	10
	20–100	$242.51 - 0.810X + 0.0065X^2$	7
300–500	0–20	$342.077X^{-0.1361}$	10
	20–100	$237.84 - 0.5957X + 0.0040X^2$	7
500–1000	0–20	$327.708X^{-0.1262} + 1.984$	15
	20–100	$230.192 - 0.4496X + 0.0033X^2$	10
1000–2000	0–20	$296.346X^{-0.0963} - 1.06$	10
	20–100	$236.786 - 0.7577X + 0.0064X^2$	10

Appendix B. Manoeuvring model and parameters

The hydrodynamic derivatives are taken from a similar inland ship in dimensions, and the detailed value under different water depths is taken from the experimental data from Koh and Yasukawa [65], which are presented in Table. B. 1.

Table. B. 1
Hydrodynamic derivatives of the inland vessel.

Symbol	$H/T = 19.3$	$H/T = 1.5$	$H/T = 1.2$	Symbol	$H/T = 19.3$	$H/T = 1.5$	$H/T = 1.2$
$X'_{\beta\beta}$	− 0.053	− 0.1749	− 0.3637	m'_x	0.006	0.0148	0.0195
X'_{rr}	0.0272	0.0792	0.1055	m'_y	0.0929	0.2325	0.3722
$X'_{\beta r}$	− 0.014	− 0.0888	− 0.248	t	0.164	0.249	0.326
Y'_{β}	0.221	0.6354	1.2375	α_H	0.194	0.089	0.418
Y'_{r}	− 0.0091	− 0.0227	− 0.113	x'_H	− 0.427	− 0.249	− 0.189
$Y'_{\beta\beta\beta}$	0.4857	2.5353	4.2245	w_{PO}	0.340	0.493	0.576
$Y'_{\beta\beta r}$	− 0.2268	0.7413	3.6005	γ_R	0.230	0.357	0.293
$Y'_{\beta rr}$	0.1562	0.286	0.7129	ℓ'_R	− 1.033	− 0.538	− 1.113
Y'_{rrr}	0.0118	− 0.0836	− 0.2003	ε	0.987	1.189	1.823
N'_{β}	0.0706	0.1988	0.4435				
N'_{r}	− 0.0593	− 0.0654	− 0.0861				
$N'_{\beta\beta\beta}$	0.0848	0.5665	1.1277				
$N'_{\beta\beta r}$	− 0.1407	− 0.6547	− 0.2249				
$N'_{\beta rr}$	0.0358	− 0.0528	− 0.0561				
N'_{rrr}	0.0028	0.0097	− 0.0522				

Regarding the bank-effect model, Figure B. 1 (a), (b) present the calculated Y_B and N_B for a vessel with a length of 100 m under a moderately shallow water condition ($H/T = 1.5$). The results cover a range of vessel speeds from 1 to 4 m/s (approximately 1.9–7.8 knots) and ship-bank distances from 1.1 to 6 times the vessel's beam. The three methods yield similar lateral attraction forces (Y_B) until the ratio of ship-bank distance to beam (d/B) becomes less than approximately 2, at which point a repulsion force appears in the model by Vantorre et al. [58]. Accordingly, Figure B. 1 (c), (d) show the detailed value from the three methods under a speed of 4 knots, where an obvious attraction force can be noticed as the vessel approaches the bank. As noted by Lataire [23], the channel wall can induce repulsion forces on the ship hull when the gap distance falls below a critical range. Therefore, this study adopts the average result of the three reference models for moderate ship-bank distances. Once a repulsion force is detected, the value from Vantorre et al. [58] will be used.

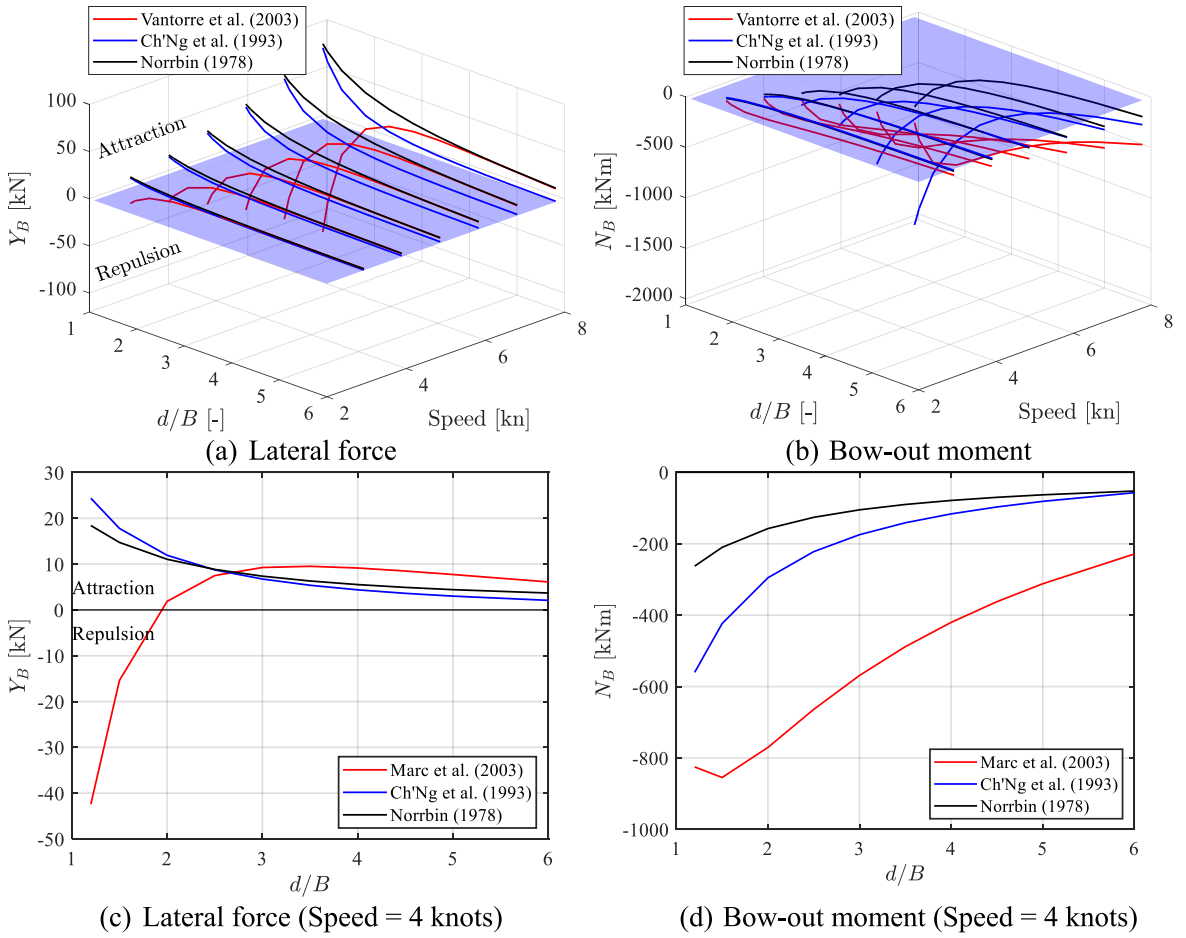

Fig. B. 1. Comparison of bank effect models under a depth-to-draught ratio of $H/T = 1.5$: (a) Overall lateral force as a function of ship-bank distance d/B and speed; (b) Bow-out moment; (c) Cross-sectional view of lateral force at 4 knots, showing the transition between attraction and repulsion zones; (d) Cross-sectional view of bow-out moment at 4 knots.

Appendix C. PSO initialisation

The parameter initialisation of the PSO algorithm for vessel energy optimisation is presented in Table. C. 1. During the iterations, the cognition of the particle (c_1), and the social influence of the swarm (c_2) follow a dynamic tuning strategy.

Table. C. 1
Initialisation parameter of the PSO algorithm

Parameters	Value
Number of particles (N)	500
Iterations (T)	50
Cognition of particle (c_1)	$c_1 = 1.6 - 0.5(t/T)$
Social influence of swarm (c_2)	$c_2 = 1.5 + 0.5(t/T)$
Maximum inertia weight (ω_{max})	0.7
Minimum inertia weight (ω_{min})	0.4

Data availability

Data will be made available on request.

References

[1] European Commission. Freight transport statistics - modal split. Available from: https://ec.europa.eu/eurostat/statistics-explained/index.php?title=Freight_transport_statistics_-_modal_split; 2023.
[2] European Environment Agency. Specific CO2 emissions per tonne-km and per mode of transport in Europe. Available from: https://www.eea.europa.eu/data-and-maps/daviz/specific-co2-emissions-per-tonne-2#tab-chart_1; 2017.
[3] Raven H. A computational study of shallow-water effects on ship viscous resistance. In: Proceedings of the 29th symposium on naval hydrodynamics, gothenburg, Sweden; 2012.
[4] Raven H. A new correction procedure for shallow-water effects in ship speed trials. In: Proceedings of the 2016 PRADS conference; 2016. *Copenhagen*.
[5] Zeng QS, Hekkenberg R, Thill C. On the viscous resistance of ships sailing in shallow water. Ocean Eng 2019;190.
[6] Norrbin NH. Bank effects on a ship moving through a short dredged channel. Naval Hydrodynamics Series; 1976.
[7] Kijima K, Nakiri Y. Prediction method of ship manoeuvrability in deep and shallow waters. 1990.
[8] Mucha P, et al. Experimental investigation of free-running ship manoeuvers under extreme shallow water conditions. Appl Ocean Res 2019;83:155–62.

[9] Pompée P-J. About modelling inland vessels resistance and propulsion and interaction vessel-waterway key parameters driving restricted/shallow water effects. Proceeding of Smart Rivers 2015, 2015:180.
[10] Zhang C, Ringsberg JW, Thies F. Development of a ship performance model for power estimation of inland waterway vessels. Ocean Eng 2023;287:115731.
[11] Sun X, et al. Analysis of the operational energy efficiency for inland river ships. Transport Res Transport Environ 2013;22:34–9.
[12] Fan A, et al. Joint optimisation for improving ship energy efficiency considering speed and trim control. Transport Res Transport Environ 2022;113:103527.
[13] Parsons DR, et al. Velocity mapping toolbox (VMT): a processing and visualization suite for moving-vessel ADCP measurements. Earth Surf Process Landf 2013;38 (11):1244–60.
[14] Yang B, Kaidi S, Lefrançois E. Numerical investigation of the parameters that may seriously impact the ship control lability in restricted bending channels. Ocean Eng 2022;266:112735.
[15] Aztjushkov L. Wall effect correction for shalow water model tests. In: Published by: the north east Coast institution of engineers and shipbuilders, bolbec hall, Great Britain, transactions, vol. 85. Russia: Leningrad Shipbuilding Institute; 1968. 2.
[16] Mucha P, et al. An experimental study on the effect of confined water on resistance and propulsion of an inland waterway ship. Ocean Eng 2018;167:11–22.
[17] Zentari L, et al. Experimental and numerical investigation of shallow water effects on resistance and propulsion of coupled pusher-barge convoys. Appl Ocean Res 2022:121.
[18] Du P, et al. Resistance and wave characterizations of inland vessels in the fully-confined waterway. Ocean Eng 2020;210:107580.
[19] Rotteveel E, Hekkenberg R, van der Ploeg A. Inland ship stern optimization in shallow water. Ocean Eng 2017;141:555–69.
[20] Islam H, et al. Propulsion power prediction for an inland container vessel in open and restricted channel from model and full-scale simulations. Ocean Eng 2021;229.
[21] Liu J, et al. Literature review on evaluation and prediction methods of inland vessel manoeuvrability. Ocean Eng 2015;106:458–71.
[22] Norrbin NH. Theory and observation on the use of a mathematical model for ship maneuvering in deep and confined water. In: Proc. 8th symposium on naval hydrodynamics; 1977.
[23] Lataire E. Experiment based mathematical modelling of ship-bank interaction. Ghent University; 2014.
[24] Nomoto K, et al. On the steering qualities of ships. Int Shipbuild Prog 1957;4(35): 354–70.
[25] Abkowitz MA. Lectures on ship hydrodynamics–Steering and manoeuvrability. 1964.
[26] Ogawa A, Kasai H. On the mathematical model of manoeuvring motion of ships. Int Shipbuild Prog 1978;25(292):306–19.
[27] Yoshimura Y. Mathematical model for the manoeuvring ship motion in shallow water. Journal of the Kansai society of naval architects; 1986. p. 200.
[28] Liu J, et al. An integrated empirical manoeuvring model for inland vessels. Ocean Eng 2017;137:287–308.
[29] Yang Y, el Moctar O. A mathematical model for ships maneuvering in deep and shallow waters. Ocean Eng 2024;295:116927.
[30] Zhang C, et al. Towards autonomous inland shipping: a manoeuvring model in confined waterways. Ships Offshore Struct 2024:1–13.
[31] He Z, et al. Dynamic domain-based collision avoidance system for autonomous ships: real experiments in coastal waters. Expert Syst Appl 2024;255:124805.
[32] Waltz M, Paulig N, Okhrin O. 2-level reinforcement learning for ships on inland waterways: path planning and following. Expert Syst Appl 2025;274:126933.
[33] Chen L, Hopman H, Negenborn RR. Distributed model predictive control for vessel train formations of cooperative multi-vessel systems. Transport Res C Emerg Technol 2018;92:101–18.
[34] Tao W, et al. Coordination and optimization control framework for vessels platooning in inland waterborne transportation system. IEEE Trans Intell Transport Syst 2022;24(12):15667–86.
[35] Xu D, et al. Path following control for large inland ships in a restricted waterway using the nonlinear terminal sliding mode method. Ocean Eng 2023;284:115159.
[36] Zheng H, Negenborn RR, Lodewijks G. Predictive path following with arrival time awareness for waterborne AGVs. Transport Res C Emerg Technol 2016;70:214–37.
[37] Mahipala D, Johansen TA. Model predictive control for path following and collision-avoidance of autonomous ships in inland waterways. In: 2023 31st mediterranean conference on control and automation (MED). IEEE; 2023.
[38] Du Z, Negenborn RR, Reppa V. Multi-objective cooperative control for a ship-towing system in congested water traffic environments. IEEE Trans Intell Transport Syst 2022;23(12):24318–29.
[39] Paulig N, Okhrin O. Robust path following on rivers using bootstrapped reinforcement learning. Ocean Eng 2024;298:117207.
[40] Zheng Q-Q, et al. Solving energy-efficient lock group co-scheduling problem with ship lift and approach channel using a collaborative adaptive multi-objective algorithm. Expert Syst Appl 2024;242:122712.
[41] Yan X, et al. Energy-efficient shipping: an application of big data analysis for optimizing engine speed of inland ships considering multiple environmental factors. Ocean Eng 2018;169:457–68.
[42] Wang K, et al. Real-time optimization of ship energy efficiency based on the prediction technology of working condition. Transport Res Transport Environ 2016;46:81–93.
[43] Fan A, et al. Decarbonising inland ship power system: alternative solution and assessment method. Energy 2021;226:120266.
[44] Guesnet T. Energy efficiency of inland water ships–and how to improve it. Inland navigation CO2 emissions-how to measure them. 2011.
[45] Hasan SR, Karim MM. Energy efficiency design index baselines for ships of Bangladesh based on verified ship data. Heliyon 2022;8(10):e10996.
[46] Fan A, et al. Comprehensive evaluation of machine learning models for predicting ship energy consumption based on onboard sensor data. Ocean Coast Manag 2024; 248:106946.
[47] Peng X, et al. The inland waterway ship emission inventory modeling: the Yangtze River case. Transport Res Transport Environ 2024;129:104138.
[48] Fan A, et al. Microscopic characteristics and influencing factors of ship emissions based on onboard measurements. Transport Res Transport Environ 2024;133: 104300.
[49] Fan A, et al. Carbon footprint model and low–carbon pathway of inland shipping based on micro–macro analysis. Energy 2023;263:126150.
[50] Wang K, et al. Computational fluid dynamics-based ship energy-saving technologies: a comprehensive review. Renew Sustain Energy Rev 2025;207: 114896.
[51] Yuan Z, et al. Prediction and optimisation of fuel consumption for inland ships considering real-time status and environmental factors. Ocean Eng 2021;221: 108530.
[52] Perera LP, Mo B. Machine intelligence based data handling framework for ship energy efficiency. IEEE Trans Veh Technol 2017;66(10):8659–66.
[53] Perez T, et al. An overview of the marine systems simulator (MSS): a simulink toolbox for marine control systems. Modeling, identification and Control 2006;27 (4):259–75.
[54] Rutkowski G. ECDIS limitations, data reliability, alarm management and safety settings recommended for passage planning and route monitoring on VLCC tankers. TransNav: International Journal on Marine Navigation and Safety of Sea Transportation 2018;12(3).
[55] Tsou M-C. Multi-target collision avoidance route planning under an ECDIS framework. Ocean Eng 2016;121:268–78.
[56] Hidouche S, et al. Ships propulsion: estimation of specific fuel consumption based on power load factor ratio. Proc., Hydrodynamics and simulation applied to inland waterways and port approaches. SHF, Société hydrotechnique de France; 2015.
[57] Ch'Ng P, Doctors L, Renilson M. A method of calculating the ship-bank interaction forces and moments in restricted water. 1993.
[58] Vantorre M, et al. Experimental investigation of ship-bank interaction forces. 2003.
[59] Breivik M, Fossen TI. Guidance laws for planar motion control. In: 2008 47th IEEE conference on decision and control. IEEE; 2008.
[60] Åström KJ, Hägglund T. PID controllers: theory, design, and tuning. Research triangle Park, North Carolina: ISA - the instrumentation, systems and automation society. 1995.
[61] Rhoads BL. River dynamics: geomorphology to support management. Cambridge University Press; 2020.
[62] Odgaard AJ. River-meander model. I: development. J Hydraul Eng 1989;115(11): 1433–50.
[63] Fossen TI. Handbook of marine craft hydrodynamics and motion control. John Wiley & Sons; 2011.
[64] Kennedy J, Eberhart R. Particle swarm optimization. In: Proceedings of ICNN'95-international conference on neural networks. ieee; 1995.
[65] Koh K, Yasukawa H. Comparison study of a pusher–barge system in shallow water, medium shallow water and deep water conditions. Ocean engineering 2012;46: 9–17.
[66] Du P, et al. Investigation on resistance, squat and ship-generated waves of inland convoy passing bridge piers in a confined waterway. J Mar Sci Eng 2021;9(10): 1125.
[67] Larrazabal JM, Peñas MS. Intelligent rudder control of an unmanned surface vessel. Expert Syst Appl 2016;55:106–17.
[68] Guarnieri M, et al. Design, construction and operation of a special electric vessel for water-city utilities service. Energy 2024;309:133110.
[69] Liu S, et al. Thermal equalization design for the battery energy storage system (BESS) of a fully electric ship. Energy 2024;312:133611.
[70] Millward A. The effect of water depth on hull form factor. Int Shipbuild Prog 1989; 36(407).
[71] Epps B, et al. OpenProp: an open-source parametric design and analysis tool for propellers. In: Proceedings of the 2009 grand challenges in modeling & simulation conference; 2009.